Cell Genomics

Article

Karyotype engineering reveals spatio-temporal control of replication firing and gene contacts

Graphical abstract

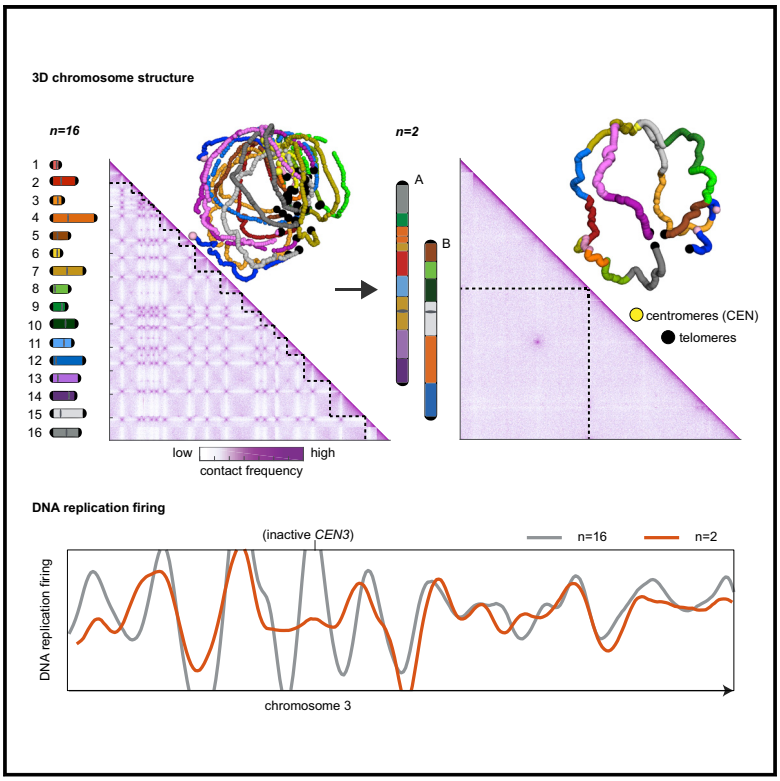

Highlights

- Nuclear size is influenced by chromosome size and their relative length
- Chromosome-core repositioning of subtelomeres unveils specific gene contacts in 3D
- Centromere inactivation delays replication firing in their vicinity
- The rDNA-centromere bridge of contacts expands over 1.5 Mb linear genomic distance

Authors

Luciana Lazar-Stefanita, Jingchuan Luo, Remi Montagne, ..., Julien Mozziconacci, Romain Koszul, Jef D. Boeke

Correspondence

romain.koszul@pasteur.fr (R.K.), jef.boeke@nyulangone.org (J.D.B.)

In brief

The work of Lazar-Stefanita et al. uses genetically engineered fused chromosomes to investigate chromosome size effect on nuclear architecture and function. The gigantic chromosomes were found to occupy more space within enlarged nuclei and maintain DNA reorganization during cell division. Site-specific, three-dimensional changes were functionally linked to temporal variations of the DNA replication program.

Lazar-Stefanita et al., 2022, Cell Genomics *2*, 100163
August 10, 2022
https://doi.org/10.1016/j.xgen.2022.100163

CellPress

Cell Genomics

CellPress
OPEN ACCESS

Article

Karyotype engineering reveals spatio-temporal control of replication firing and gene contacts

Luciana Lazar-Stefanita,[1,2] Jingchuan Luo,[1,5,6] Remi Montagne,[2,5,7] Agnes Thierry,[2] Xiaoji Sun,[1,8] Guillaume Mercy,[2,9] Julien Mozziconacci,[3] Romain Koszul,[2,*] and Jef D. Boeke[1,4,10,*]

[1]Institute for Systems Genetics and Department of Biochemistry and Molecular Pharmacology, New York University Langone Health, New York, NY 10016, USA

[2]Institut Pasteur, CNRS UMR3525, Université Paris Cité, Spatial Regulation of Genomes Unit, 75015 Paris, France

[3]Structure and Instability of Genomes Lab, UMR 7196, Museum National d'Histoire Naturelle, Paris, France

[4]Department of Biomedical Engineering, New York University Tandon School of Engineering, Brooklyn, NY 11201, USA

[5]These authors contributed equally

[6]Present address: Whitehead Institute for Biomedical Research, Cambridge, MA 02142, USA

[7]Present address: Institute Curie, 26 rue d'Ulm, 75005 Paris France

[8]Present address: Cellarity, Cambridge, MA, USA

[9]Present address: Fondation Hospitalière de France, 1 bis Rue Cabanis, 75014 Paris, France

[10]Lead contact

*Correspondence: romain.koszul@pasteur.fr (R.K.), jef.boeke@nyulangone.org (J.D.B.)

https://doi.org/10.1016/j.xgen.2022.100163

SUMMARY

Eukaryotic genomes vary in terms of size, chromosome number, and genetic complexity. Their temporal organization is complex, reflecting coordination between DNA folding and function. Here, we used fused karyotypes of budding yeast to characterize the effects of chromosome length on nuclear architecture. We found that size-matched megachromosomes expand to occupy a larger fraction of the enlarged nucleus. Hi-C maps reveal changes in the three-dimensional structure corresponding to inactivated centromeres and telomeres. De-clustering of inactive centromeres results in their loss of early replication, highlighting a functional correlation between genome organization and replication timing. Repositioning of former telomere-proximal regions on chromosome arms exposed a subset of contacts between flocculin genes. Chromatin reorganization of megachromosomes during cell division remained unperturbed, and it revealed that centromere-rDNA contacts in anaphase, extending over 0.3 Mb on wild-type chromosome, cannot exceed ~1.7 Mb. Our results highlight the relevance of engineered karyotypes to unveiling relationships between genome organization and function.

INTRODUCTION

Over billions of years of evolution, genomes have acquired distinct characteristics. In eukaryotes, chromosome size, number, and structural organization within the nuclear space are diverse, reflecting a history of dynamic evolutionary changes. The 12-Mb budding yeast genome, distributed among 16 chromosomes, encodes ~6,000 genes.[1] By contrast, flies, worms, and humans have much larger genomes (8–250 times as large as yeast, distributed across 4, 6, and 23 pairs of chromosomes, respectively), but only carry 2–3 times as many genes as yeast do. This indicates a lack of strong functional correspondence between genome size, chromosome number, and gene content.[2] Nevertheless, DNA content has been linked to a number of phenotypic traits: its increase is concomitant with the cell size across a wide variety of taxa while it correlates inversely with the rate of cell division. Hence, a high DNA content is typically found in nuclei of large and slowly dividing cells.[2,3]

Imaging and chromosome conformation capture (3C; Hi-C) studies have revealed complex architectures. Distinct nuclear territories of various sizes occasionally interact with one another; yeast centromeres and telomeres cluster into discrete foci, whereas the nucleolus occupies a distinct territory opposite the spindle pole body (SPB).[4] Ergo, the DNA molecule is not strictly informational, but can also structure the nucleus. Nuclear repositioning has been linked to local gene regulation in yeast,[5,6] and highly transcribed genes result in boundaries in chromosome contact maps delimiting small microdomains along interphase chromosomes.[7,8] As yeast cells enter mitosis, their chromosomes are reorganized into arrays of relatively small (~10–40 kb) chromatin loops, mediated by the cohesin complex.[9–13] The mechanism of cohesin-mediated loops is conserved in mammals, where they maintain large topologically associating domains (TADs) in interphase.[14–17]

Here, we deploy a new strategy to investigate nuclear DNA architecture and function on karyotype-engineered yeasts that carry megachromosomes produced by sequential rounds of telomere to telomere fusion and simultaneous removal of one centromere.[18,19] These genomes, which carry massive "designer rearrangements," represent new resources for

investigating functional consequences of genome three-dimensional (3D) restructuring. We show that inactivation of pericentromeric regions during megachromosome engineering modifies the higher order organization and abolishes their early replication firing, demonstrating a functional link between overall genome organization and regulation of replication. Likewise, reposition of formerly telomere-proximal regions along megachromosome arms reveals unexposed interactions between discrete chromosomal sites that evaded detection in the native yeast genome. Despite that the relative size of the fused megachromosomes was found to differentially affect nuclear size, initial studies revealed a surprising lack of major fitness defects, pointing to a resilient genome structure that strongly argues against the idea that intranuclear position is a major determinant of gene expression.[18–20] In addition, the mitotic characteristics of native chromosomes are maintained in megachromosomes, showing that chromosome length regulates neither chromatin compaction nor segregation efficiency, underscoring the robustness of mitosis in yeast. These results reinforce the relevance of local 3D nuclear architecture on genome structure and function and highlights the importance of finding alternative ways to investigate it.

RESULTS

Size-matched versus unmatched megachromosomes

Yeast strains carrying massively reorganized karyotypes have been engineered and thoroughly described.[18,19] Briefly, these studies showed that chromosome size can be massively increased through multiple rounds of telomere-telomere fusion and simultaneous centromere deletion (to prevent the formation of dicentric chromosomes) without incurring major fitness defects.

The present work focuses on yeasts whose 16 native chromosomes have been sequentially merged into 2 final megachromosomes (Figures 1A and S1A), which, for the sake of clarity, we named alphabetically from the largest to the smallest (e.g., chrA and chrB) in each strain. In earlier work by Luo et al.,[18] we described an n = 2 strain, JL402, with two approximately equal size chromosomes. Here, to further investigate the potential importance of the "size-matched" chromosomes, we designed and constructed an "unmatched" n = 2 karyotype, in which one chromosome is 3 times larger than the other (Figure S1A). Interestingly, the unmatched n = 2 strain (JL498) has a severe growth defect relative to the size-matched strain (Figure S1B). Additional studies were performed on two n = 3 strains (JL381 and JL410; growth rates reported by Luo et al.[18]) that served as progenitors of the two n = 2 strains (Key resources table; Figure S1A).

Transcriptional regulation is affected in the size-unmatched n = 2

We previously showed that the transcriptome of the size-matched n = 2 strain is not severely changed compared to n = 16, and was mostly attributed to the relocation of previously telomeric genes to internal chromosomal arm locations.[18] We analyzed RNA sequencing (RNA-seq) libraries of the n = 2 size-unmatched strain (Method details), which has a stronger growth defect compared to n = 2 size-matched (Figure S1B). Consistent with the slow growth phenotype, we detected hundreds of differentially expressed genes (DEGs; log2 fold change >2 or <−2 and $p < 1E10^{-5}$); however, no coherent pattern of gene ontology (GO) term enrichment could be identified among those DEGs (Figure S2; Tables S1–S3). The transcription of the former pericentromeric genes, located ∼20 kb upstream and downstream of the inactivated centromeres, remained largely unaffected and independent of chromosome size, suggesting that transcription is not influenced by centromere positioning nor the structure of the pericentromeric chromatin. The disturbed transcriptome of the n = 2 unmatched strain could be directly related to its slow growth phenotype. Alternatively, it is possible that one or more novel mutations, which are absent from the size-matched strain, arose in the unmatched affecting its fitness.

3D nuclear organization of megachromosomes

We reasoned that a ∼5-fold increase in chromosome length, relative to the longest native chromosome, may alter nuclear occupancy of the megachromosomes. To investigate this hypothesis, we started by measuring the surface area occupied by the genomic DNA in cells labeled with SYTOX Green (Method details). Our results showed an increase of ∼26% in DNA occupancy in the n = 2 size-matched compared to n = 16 (Figure 1B), which was undetected in the n = 2 unmatched strain (Figure S3; Table S4). Finally, the increase in DNA occupancy in the n = 2 size-matched was directly correlated with a ∼25% enlargement of the nuclear surface itself (Figure S5; Table S5). These results suggest a link between the size of the nucleus and the size of chromosomes. However, it remains unknown how only the size-matched megachromosomes but not the unmatched ones have this effect on nuclear size.

To characterize the spatial organization of megachromosomes, Hi-C experiments were performed on G1 synchronized n = 16 and n = 2 cells (Method details). In contrast to the contact map of the reference strain with 16 chromosomes, which displayed a characteristic 15-spot off-diagonal pattern reflecting centromere clustering associated with contact enrichment between pericentromeric regions,[22] the n = 2 map displays only 2 long chromosomes and a single off-diagonal spot of inter-pericentromeric contacts (Figure 1C). Although 2D maps and the corresponding 3D representations of n = 2 and n = 16 are highly distinct (Figures 1D and S6), the key known architectural elements of yeast nuclear organization remain conserved and independent of chromosome length. Most noticeable are the *trans* contacts between the remaining active centromeres (Figures 1C, black arrowheads, and S6), reflecting their clustering adjacent to the SPB (yeast microtubule organizing center), as well as telomere clustering.

Chromatin folding is independent of chromosome size

We expected that the process of chromosome fusion would alter the overall balance between intra- and inter-chromosomal contacts, that we evaluated by quantifying their relative contact percentages in the 2D maps of both n = 2, size-matched and unmatched strains, and compared to n = 16. A gain of up to ∼30% of intrachromosomal contacts was observed in n = 2 strains (Figure S7A). We next asked whether this increase could affect the internal structure of megachromosomes during G1 compared to their n = 16 counterparts. Modifications of chromatin folding can be assessed, to some extent, by computing the contact probability *p* as a function of the genomic distance

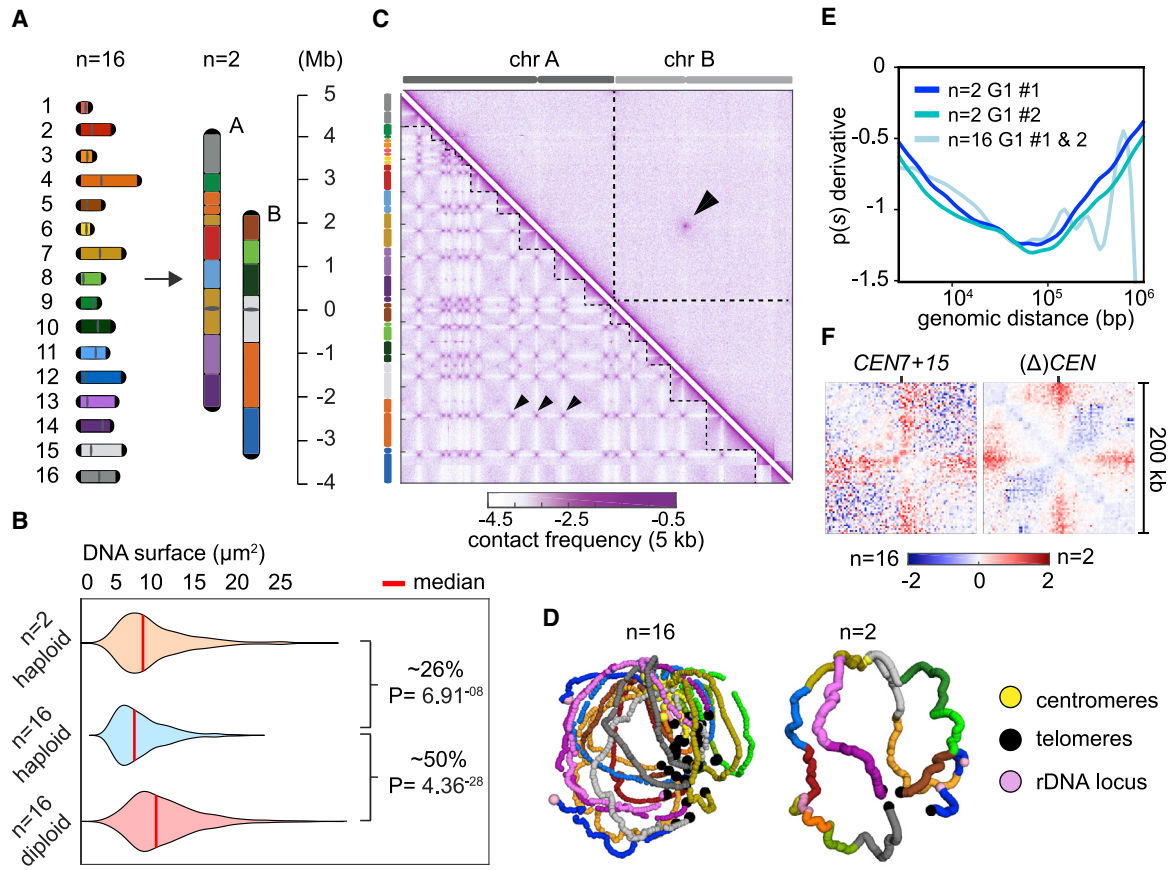

Figure 1. Genome structure of 2 megachromosomes

(A) Overview of the chromosome fusion design from n = 16 to n = 2. The 16 native chromosomes are uniquely colored and ordered numerically, while the 2 fused megachromosomes are alphabetically ordered (A and B). Length of chromosome arms is indicated as a function of distance from the centromere position (Mb).

(B) Measurements of DNA surface (μm^2) in cells stained with SYTOX Green. Violin plots display: Median values of DNA surface in haploid (n = 16 and n = 2) and diploid (n = 16, positive control for size increase) strains, and their relative (%) increments when compared to n = 16 haploid. p values obtained through Kolmogorov-Smirnov test.

(C) Contact map comparison of n = 16 and n = 2 in G1 phase. Left and right Hi-C maps (5 kb binned) were generated by aligning both n = 16 and n = 2 reads on a reference sequence containing only 2 chromosomes. Bottom left map shows all 16 native chromosomes underlined by dotted lines, while the top right map displays only 2 chromosomes (chrA and chrB, atop the map). Black arrowheads point to inter-pericentromeric contacts. Violet to white color scale reflects high to low contact frequencies (log10).

(D) 3D average representations of G1 contact maps of n = 16 and n = 2. Color code reflects the 16 native chromosomes, and centromeres, telomeres, and rDNA are highlighted.

(E) *p*(*s*) derivative represents the average decay of the intra-chromosomal contact frequency *p* between loci with respect to their genomic distance *s*. Two G1 replicates of both n = 16 from Lazar-Stefanita et al.[21] and n = 2 were plotted together.

(F) Cumulative log ratios of active and inactivated pericentromeric regions. Blue to red color scale reflects contact enrichment in 200-kb windows in n = 2 versus n = 16 (log2).

(*s*) along chromosome arms.[21,23] Because chromosome size is considerably enlarged in n = 2 compared to n = 16 strains, a direct comparison between their *p*(*s*) curves is made problematic by the high variation in the inter-/intra-contact ratio between the 2 genomes. To address this issue, we computed the *p*(*s*) in 300-kb windows over the chromosomes of both strains (Method details). No significant differences were detected along the megachromosomes compared to native ones in G1 in this local analysis (Figure S7B). We then calculated the local derivative of the full *p*(*s*) curve in log-log space for both n = 16 and n = 2 genomes to magnify their differences[9,24] (Method details). For the most part, the derivatives displayed similar slopes, with the exception of long distances (>150 kb), as small chromosome arms introduce variability in the n = 16 plot (Figure 1E). This result indicates that within the nuclear space, the long chromosomal arms of fused strains display an average chromatin folding state similar to that of the 32 shorter arms in G1.

Centromere inactivation leads to the reorganization of the pericentromeric chromatin

Due to centromere clustering, chromosomal arms adopt a "polymer brush"-like conformation[25] that leads to local contact variations around centromere positions in both *cis* and *trans*.[26,27]

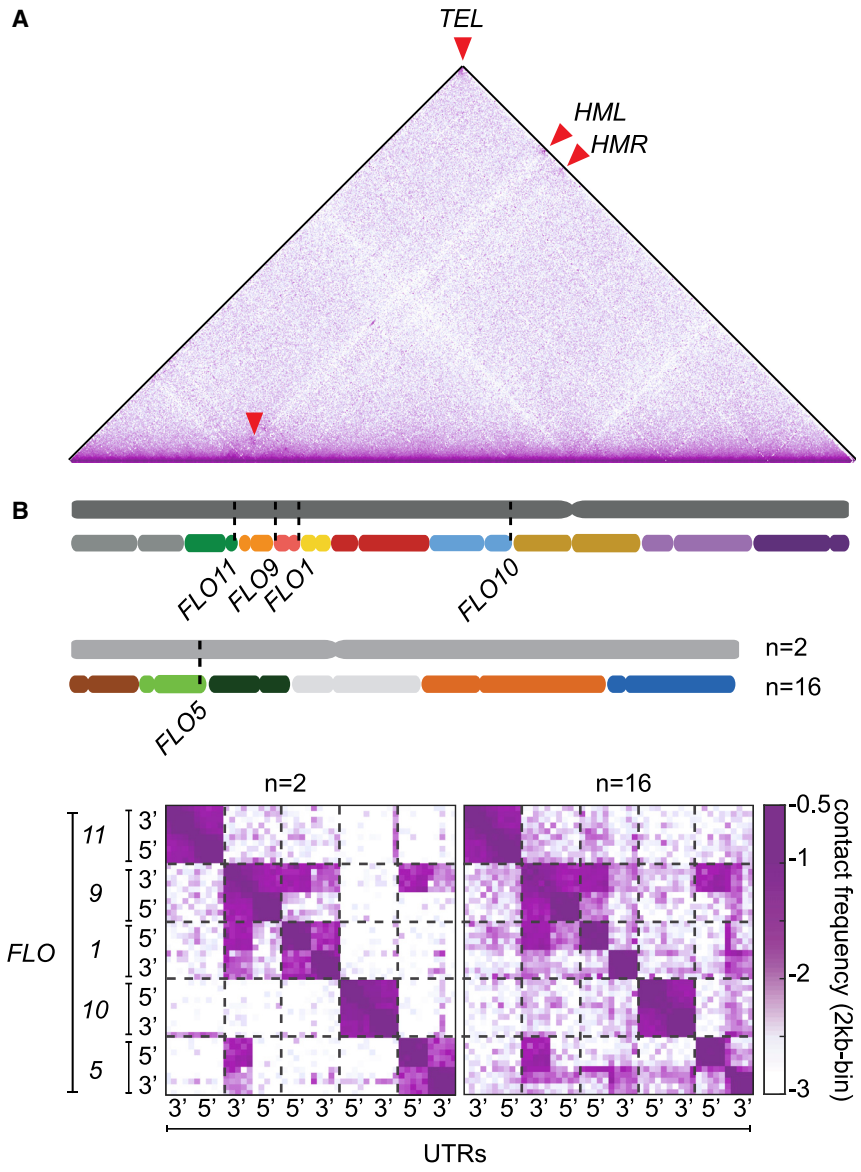

Figure 2. Repositioning of subtelomeric genes internally to chromosomal arms reveals their contact in 3D

(A) Contact map of chrA in n = 2 (5 kb-binned). Red arrowheads point at *cis* contact enrichment between *HML*, *HMR*, and *TEL*. Violet to white color scale reflects high to low contact frequencies as in Figure 1.

(B) Dotted lines indicate locations of the *FLO* genes both on n = 2 and n = 16 chromosomes. Contact maps of unique *FLO*-flanking regions in n = 2 and n = 16 (2 kb-binned). y and x axes indicate gene name and the orientation of the unique 10-kb sequences flanking the *FLO*5′ and-3′ UTRs) in the n = 2 genome. The resulting 20-kb regions adjacent to each gene are underlined by dotted lines.

Given that the number of active centromeres in n = 2 is reduced 8-fold compared to n = 16, we thought that this may affect the brush structure, which is known to depend on the grafting density (e.g. the number of polymer end per unit area [4 for n = 2 karyotype, compared to 32 for n = 16 karyotype]).[28] A decreased polymer brush effect was observed in n = 2 contact maps when compared to n = 16, as highlighted in the log ratios maps between 200-kb regions from n = 2 and n = 16 strains centered on either the retained active centromeres *CEN7* and *CEN15* or the inactivated ones (Figure 1F). In the n = 2 strain, the four pericentromere regions around *CEN7* and *CEN15* engage in longer range contacts than in the n = 16 strain (red stripes), as they become unconstrained by the loss of the brush-like effect. The chromatin flanking the 14 inactivated centromeres completely lose the polymer brush conformation (Figure S7C, log2-ratio maps). In other words, the larger the collective bulk of centromeric sequences at the kinetochores, the higher their degree of insulation.

Telomere deletion reveals inter- and intra-chromosomal FLO gene contacts

In yeast, heterochromatin is observed at and near the 32 telomeres and at the 2 silent mating type loci, *HML* and *HMR*, located near the left and right telomere of chromosome 3, respectively.[4] These heterochromatic loci are thought to co-localize, forming subnuclear compartments enriched in silencing proteins Sir2-3-4.[29] As each chromosome fusion deletes two telomeres and relocates the subtelomeric regions internal to a chromosome arm, it was not surprising to observe that the 28 formerly subtelomeric regions in the n = 2 strain stopped being in contact. However, the 2D maps revealed that a subset of these regions continued to exhibit discrete contacts (Figure 2). Among these contacts were the mating type loci (*HML* and *HMR*) with the retained subtelomeres (Figure 2A, red arrowheads), probably a result of their Sir3-dependent anchoring to the nuclear envelope.[30] In addition, a set of distinct contacts involving three loci, formerly positioned within subtelomeric regions, appeared on the fused chromosomal maps. These previously unexposed contacts correspond to members of the *FLO* gene family, a co-regulated set of genes that trigger yeast flocculation in response to adverse conditions.[31] *FLO1*, *5*, *9*, *10*, and *11* are telomere-adjacent (~10–40 kb) genes encoding 5 cell-wall glycoproteins or flocculins.[32] The expression of the flocculins is regulated both genetically and epigenetically, through recombination[33,34] and histone deacetylase-mediated silencing, respectively.[35] To eliminate the possibility that these contacts correspond to sequence misalignments due to the repetitive nature of the genes, we masked their repetitive components and investigate contacts only between the unique regions flanking these genes (Method details; Figure S8). The contact maps binned at 2-kb

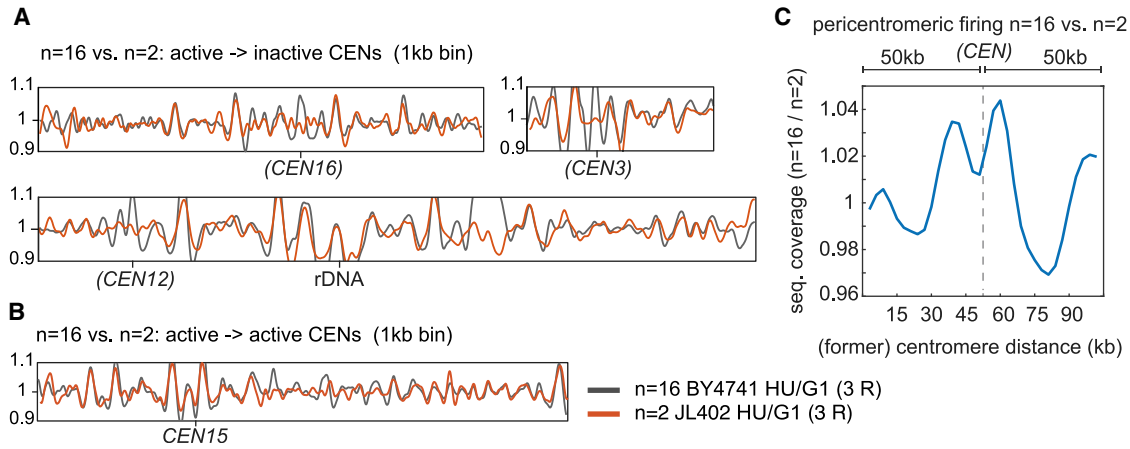

Figure 3. 3D de-cluster of inactive centromeres delays their replication timing

Each replication timing plot[41,42] in (A) and (B) is the average representation of 3 independent replicates and shows the sequencing coverage ratio of S phase (HU) synchronized cells normalized on the G1 (α-factor) non-replicating cells (1 kb-binned). Replication timing profiles of the n = 16 (BY4741) are shown in gray, while those of n = 2 size-matched (JL402) are in orange.

(A) Representative comparison profiles of chromosomes with inactive centromeres in n = 2, but active in n = 16 (brackets).

(B) Comparison profiles of chromosome 15 with active centromere in both n = 2 and n = 16.

(C) Pericentromeric firing in n = 16 versus n = 2. The ratio plot shows the early firing of pericentromeric regions (~100 kb) in n = 16 in respect to n = 2, in which centromeres were inactivated. Centromere position appears in brackets and is indicated with a dotted line.

windows display interactions between all 10-kb regions adjacent to either the 5′ or 3′ UTR of each *FLO* gene (Figure 2B). Surprisingly, the 3′ UTR flanking region of *FLO9* engages in strong *cis* contacts with both regions adjacent to *FLO1* and in *trans* contacts with a third position located at the *FLO5* 5′ UTR (Figure 2B). The same pattern of contacts was also observed in other fusion strains and is further illustrated by 4C-like analysis (Figure S9). Finally, a closer inspection of the n = 16 contact map reveals their presence in the wild-type yeast chromosomes, where they are largely masked by the contact signal resulting from telomere clustering (Figure 2B).

Megachromosomes therefore unveil contacts between these functionally related genes, which were difficult to observe in wild-type n = 16 strains due to their original subtelomeric position. Whether the *FLO* genes are actively clustered (and why), or whether these contacts are an indirect consequence of nuclear envelope targeting of silenced chromatin remains unknown. No additional intra- and inter-arm off-diagonal contacts were detected in the n = 2 contact maps, suggesting that robust *trans* contacts in the yeast genome are rare.

Structural and functional outcomes of 3D megachromosome organization

Spatiotemporal alteration of the DNA replication program

Replication of eukaryotic chromosomes is regulated both spatially and temporally. In yeast, replication initiates at ~260 discrete origins, which are classified according to their firing time (early or late).[36] The resulting replication program is regulated by limiting amounts of pre-replication complex factors that are recruited preferentially to early origins during early S phase and recycled to late origins throughout S phase. Replication factors are preferentially recruited to pericentromeric origins by their interaction with kinetochore components and to non-pericentromeric origins by forkhead transcription factors.[37,38] This observation was proposed to account for the early firing of origins located in the vicinity of centromeres (spanning as much as 100 kb).[37,39]

Given that the former pericentromeric regions of inactive centromeres lose their spatial proximity to the SPB in the megachromosome strains, this new configuration provided an opportunity to directly test the interplay between genome organization and replication timing. Flow cytometry of DNA contents of cells synchronized in G1 with α-factor and released into S phase showed a delay in n = 2 compared to n = 16 (Figure S10; Method details). A prolonged S phase suggested a potential lower number of early replicated regions in n = 2. To test this hypothesis, we computed the replication profile as well as origin mapping using marker frequency analysis (MFA) approaches.[40] n = 2 and n = 16 cells were arrested in G1 using α-factor and released synchronously into S phase in the presence of 200 mM hydroxyurea (HU) (Figure S11; Method details). HU treatment induces deoxynucleoside triphosphate (dNTP) starvation that results in the early S phase arrest. The mapping of early firing origins was done by computing chromosome sequence coverages in S phase that were normalized to G1 (unreplicated) and plotted along the reference genome at 1-kb resolution (Figures 3A, 3B, S12, and S13). In parallel, the replication timing profiles were generated from asynchronous cultures normalized to G1 read coverage (Figure S14).[40] Replication timing profiles and origin mapping of homologous regions in n = 2 and n = 16 remained highly conserved along chromosomal arms. However, both plots displayed differences near the former pericentromeric positions in n = 2 compared to n = 16, with a loss of early firing in regions flanking the inactive centromeres (Figure 3A, brackets), whereas the replication of active centromeres remained unaffected

(Figure 3B). A quantification of this effect is illustrated in the firing ratio of the active pericentromeres (n = 16) versus the inactive (n = 2) within 100-kb centromere-flanking regions (Figures 3C and S15). These results reinforced the essential role of the ~125-bp centromere sequence in defining early firing and provides direct evidence of the 4D regulation of the replication program in yeast, with the SPB-centromere-kinetochore complex titrating essential components for origin firing and acting as an "early replication factory."[11]

Mitotic folding and segregation

After replication, the two sister chromatids (SCs) must be equally distributed during mitosis in the two daughter cells. In metaphase, the structural maintenance of chromosomes (SMC) cohesin complex not only holds SCs together but also promotes compaction through the formation of chromatin loops along their lengths.[10–12] Cohesins are subsequently released, while the SMC condensin complex promotes chromosome segregation during anaphase.[11,43–46]

The n = 2 strain enables the investigation of chromosome size effect on metaphase and anaphase chromosome structures. Hi-C experiments of n = 2 size-matched were performed in metaphase-arrested cells using nocodazole, and late-anaphase arrest using a thermosensitive allele (*cdc15-2* t45) (Method details). Comparisons of contact maps and frequency *p*(*s*) show that megachromosomes undergo a cell-cycle-dependent reorganization similar to n = 16 chromosomes (Figures 4A and S16–S18).

Given the high degree of sequence similarity between n = 2 and n = 16 strains (>99.9%, not counting deletions of subtelomeres), we speculated that the sites of SMC enrichment would be conserved. To verify this hypothesis, we computed log ratios of pile-up plots that display the Scc1 cohesin deposition pattern[47] during metaphase compared to non-cohesin sites in 80-kb windows (Method details).[24,48] The pile-up displayed conserved patterns of contact enrichment at cohesin sites in n = 2 and n = 16 from G1 to anaphase (Figures 4B and S16, top panel), suggesting that cohesin distribution on metaphase chromosomes was chromosome size independent. In addition, cohesion loop scores computed using *Chromosight*[49] were similar in n = 16 and n = 2 strains (Figure S16, bottom panel).

In a previous work, we showed that during yeast anaphase, a specific type of SMC complex, the condensin, mediates contact enrichment between the rDNA and the pericentromeric regions of the 16 chromosomes of wild-type yeast.[21] We hypothesized that condensin-mediated loop extension would promote, directly or indirectly, the formation of a large (~300 kb) loop/domain on chr12 between the two putative "roadblocks," the nucleolus and the centromere (*CEN12*). In this work, we took advantage of the increased distance between the rDNA and the centromere to measure the size of this potential loop/domain of contacts within megachromosomes. As a consequence of chromosome fusion, the rDNA-centromere distance was increased by 5- to 10-fold in n = 3 (LS381) and n = 2 (size-matched, strain: LS402) fused strains (Key resources table), respectively. The extension of the rDNA-CEN contact domain was measured by comparing 2D maps obtained from n = 16, n = 3, and n = 2 cells arrested in either G1 (when no contacts are expected) or in late anaphase using the *cdc15-2* allele (rDNA-CEN contacts are expected). In all of the strains, the ratio maps showed an increase in short-/medium-range contacts that span from the left-flanking region adjacent to the rDNA locus toward the centromere, reaching up to ~1.7 Mb in n = 2 (Figures 4C and S18). In n = 3, the rDNA-CEN contacts extend over the entire 1.5-Mb enclosed region, whereas in n = 2, where the rDNA-CEN distance is 2.8 Mb, the intensity of contact enrichment emerging from the rDNA gradually decreases and eventually vanishes at approximately 1 Mb from the centromere without forming a clear chromatin boundary. These results suggest that the condensin-mediated loop/domain is highly dependent on the rDNA locus, which appears to represent a fixed roadblock that could, for instance, provide a reservoir of condensins that may extrude chromatin loops while moving toward the centromere. The 3D representations of the contact maps show no loop formation between the centromere and the rDNA in n = 2 (Figure 4D). Therefore, we concluded that the structural transitions of chromatin known to occur during the cell cycle are conserved in the megachromosomes.

DISCUSSION

In this work, we investigated the regulation of chromosome folding of yeast strains whose genomes carry massive chromosome fusions. The normal karyotype of yeast (containing 16 chromosomes, n = 16) was reduced up to 8 times (in n = 2) through serial telomere-telomere fusions and centromere deletion.[18] During this process, the size of the relatively small yeast chromosomes was dramatically increased. Megachromosomes represent a unique resource to investigate aspects of nuclear architecture using Hi-C, independently of the reverse genetics approach. The Hi-C protocol, especially the crosslinking step, favors *cis* over *trans* contacts.[50] As a result, the underrepresented *trans* contacts may be overlooked in the Hi-C analysis.[51] Therefore, we reasoned that this technical limitation could at least partially be circumvented in the fused genomes where many *trans* contacts became *cis*. It is worth noticing that this simple working model does not account for contact variability that may result from differences in chromatin properties, when loci in *trans* are repositioned in *cis,* nor the increased chromosome length. These are potential factors that may play key roles in their contact detection. Chromosome organization of a distinct but related fusion configuration was recently studied using a similar approach.[19] However, this study was performed in asynchronous cells and did not address some functional aspects of these novel 3D genome organizations. Here, we tackle this question and compare two n = 2 strains with size-matched versus unmatched versions of megachromosome and characterize their properties compared to the regular n = 16 parental genome.

Nuclear occupancy and genome organization of fused karyotypes during the cell cycle

We observed that size-matched megachromosomes occupy a larger fraction of the total nuclear space than do standard chromosomes. Why this trend was not seen in the unmatched megachromosome strain remains unknown. We can only speculate that cells are able to perceive total number and length of

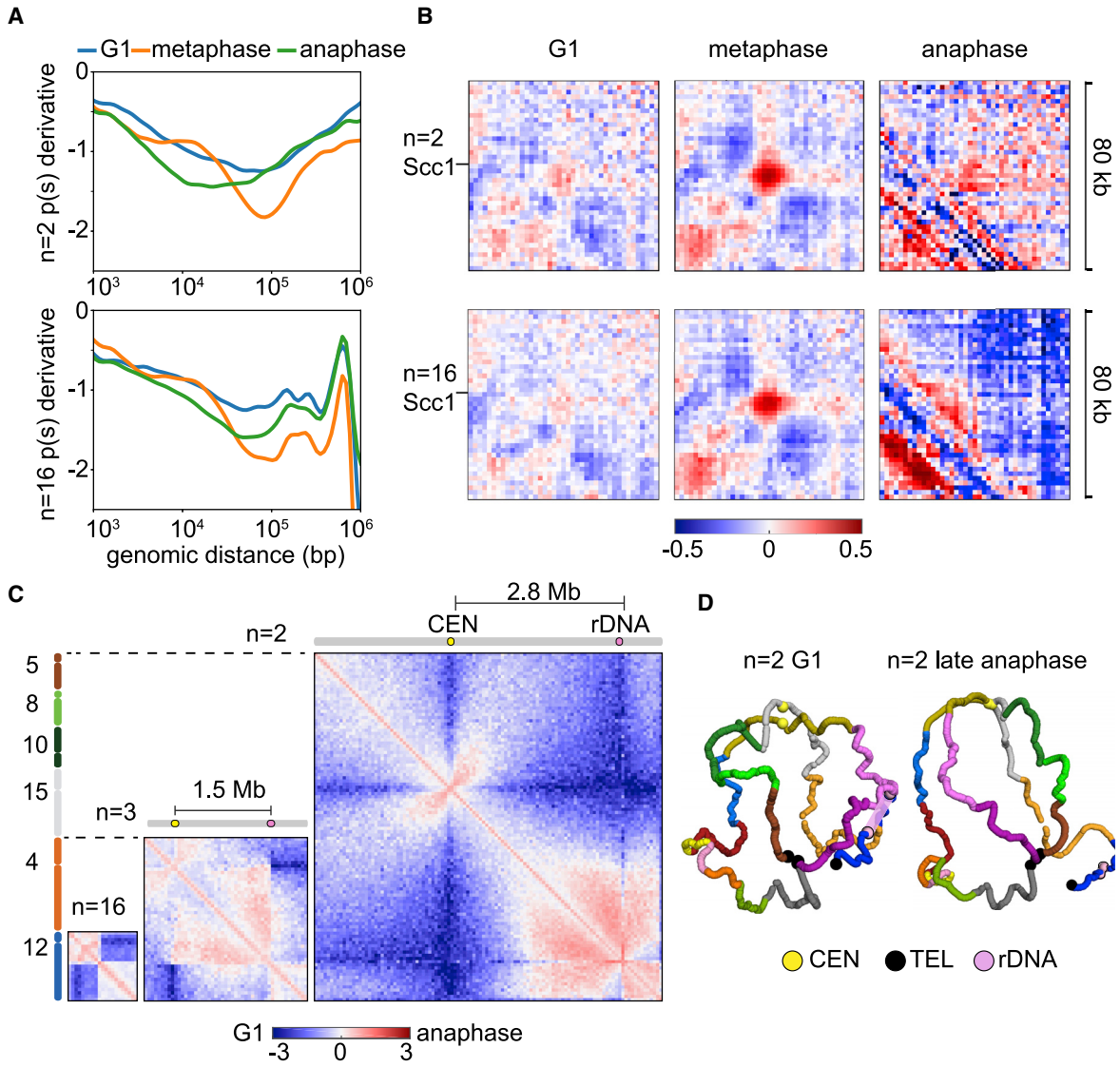

Figure 4. Cell-cycle reorganization of the megachromosomes

(A) *p*(*s*) derivatives of G1, metaphase, and anaphase synchronized cells. Top and bottom panels display slope decays along n = 2 chromosomes and n = 16 chromosomes, respectively (Hi-C data relative to n = 16 from Dauban et al. and Lazar-Stefanita et al.[9,11]).

(B) Pile-up ratio plots of 80kb windows (2-kb bins) centered on pairs of Scc1-enriched or randomly chosen positions during G1, metaphase, and anaphase. Ratios are ordered according to the distance between Scc1 binding sites in n = 2 and n = 16 strains. Blue to red color scale indicates contact enrichment between Scc1 binding sites compared to random genomic positions (log2).

(C) Centromere-rDNA contacts extend over Mb distance in fused genomes. Comparison of log-ratio contact maps between G1 and anaphase in n = 16, n = 3, and n = 2 (50 kb-binned). Size of the chromosome and centromere-rDNA distance increase progressively from left to right contact maps. Centromere (yellow) and rDNA (pink) positions, as well as their relative distances (Mb), are indicated at the top of the maps. Blue to red color scale reflects contact enrichment in anaphase compared to G1 (log2). For clarity, n = 16. Data reproduced from Lazar-Stefanita et al.[21]

(D) 3D average representations of n = 2 G1 and anaphase contact maps. Color code reflects the 16 native chromosomes, and centromeres, telomeres, and rDNA are highlighted.

chromosomes and regulate their nuclear volume accordingly. One hypothesis is that the size discordance between the two unmatched megachromosomes (~3 versus ~9 Mb) is not efficient to induce a nuclear increase as in the size-matched cells. Further studies are required to test this hypothesis and the molecular mechanisms involved in this chromosome-nucleus communication. Furthermore, the n = 2 unmatched strain also contained a larger population of cells carrying excess DNA content compared with the size-matched n = 2 and n = 16 strains (Figure S4), consistent with a slight increase in autopolyploidization, which was mainly observed by sensitivity to canavanine (toxic analog of arginine). Given these observations we speculate that a size-matched karyotype in the context of a reduced chromosome number is required to maintain ploidy.

We have shown that the structure of chromatin and its dynamic reorganization during the cell cycle is maintained independently of fused chromosome length. In addition, key landmarks of yeast chromosome configuration, such as centromere and telomere clusters, were conserved throughout the entire cell cycle. These results agree with the retained contact enrichment among Scc1 binding sites genome-wide along the large chromosomes, suggesting that SMC deposition is independent of the length of the DNA molecule. This conservation in G2/M cohesin-dependent folding suggests that the length of the condensed yeast chromosomes does not affect their segregation. Instead, condensin-mediated pulling of chromatin is likely to be the main driving force promoting efficient segregation of the genetic material between daughter cells in M phase.[52]

Finally, the fused chromosomes allowed assessment of the potential expansion of the condensin-dependent CEN-rDNA anaphase loop, reported on chr12 of wild-type yeasts.[11,53] We show that in mitosis, the centromere and rDNA contact each other over distances that do not exceed 1.7 Mb. Our hypothesis is that condensins may extrude DNA loops of various sizes that gradually merge but, eventually, unload from the chromosome before they reach the other major condensin loading center and/or roadblock, the centromere. A similar scenario was envisioned during dosage compensation of the X chromosome in *Caenorhabditis elegans*.[54]

Effects on centromeres and telomeres

We show that, despite the tremendous increase in the size of the chromosomes, the better known aspects of yeast chromosome folding are overall preserved in n = 2 genomes. However, local contact variations, especially surrounding the inactivated centromeres and deleted telomeres, were observed. Relocation of formerly pericentromeric and subtelomeric regions to internal chromosome arm positions revealed direct functional aspects associated with their 3D localization. Centromeres have long been known to be early-replicating regions.[39,55,56] Their temporal regulation was shown to depend on preferential recruitment of a limiting pre-replication factor, Dbf4, at pericentromeres through its physical interaction with Ctf19, a kinetochore component.[38,39] Consequently, it was proposed that origins located in the immediate vicinity of centromeres fire early because of their Dbf4 enrichment. Here, we showed that the structural inactivation of centromeres (some of which were limited to 3-bp deletions; see detailed design by Luo et al.[18]) leads to the loss of early firing in their environs. Therefore, our results are consistent with the suggestion that the centromeres cluster acts as a replication factory that titrate limiting factors to ensure synchronous firing of pan-chromosome replication.

We also unveiled interactions involving a subset of heterochromatin-prone loci and members of a functionally related gene family, the *FLO* genes. Contacts between the silent mating type loci *HML* and *HMR* and the distant remaining telomeres were also shown in our earlier work to depend on the silencing complex, SIR.[30] Here, we describe additional contacts between *HML* and *FLO10* (Figure S9), another Sir-dependent complex.[35] *FLO10* is a member of the flocculin gene family encoding cell-surface glycoproteins (*FLO1*, *5*, *9*, *10*, and *11*) that confer adherence to agar, solid surfaces, and other yeast cells. *FLO* genes are subtelomeric, a location suggested to play important roles in their evolution.[33,57] We have shown that *FLO*s and their flanking sequences remain in contact with one another both in *cis* and in *trans*, revealing their intrinsic ability to co-localize, even when no longer subtelomeric. As these genes are not expressed in our strains,[58] we speculate that their co-localization is independent of their functional activity and may be linked to their epigenetic silencing. It is noteworthy that *FLO1* and *FLO5*, found to be in spatial proximity with *FLO9*, were both deleted in the design of the single chromosome karyotype n = 1, published by Shao et al.[19] As a matter of fact, neither we nor the authors of this latter work were able to detect contacts between the flanking regions of these genes that were partially retained after their deletion.

In summary, studies of megachromosomes have revealed a wealth of new information about the plasticity of genome organization, control of nuclear volume and DNA replication, and previously undetected interchromosomal contacts.

STAR METHODS

Detailed methods are provided in the online version of this paper and include the following:

- KEY RESOURCES TABLE
- RESOURCE AVAILABILITY
  - Lead contact
  - Materials availability
  - Data and code availability
- EXPERIMENTAL MODEL AND SUBJECT DETAILS
- METHOD DETAILS
  - Media and culture conditions
  - Spot assays
  - Pulsed-field gel electrophoresis
  - DNA staining
  - Imaging DNA occupancy and nuclear size
  - Cell cycle progression
  - Cell synchronization
  - Hi-C: Library preparation
  - Hi-C: Data processing
  - Replication timing
  - RNA-seq
  - Genome annotation
- QUANTIFICATION AND STATISTICAL ANALYSIS

SUPPLEMENTAL INFORMATION

Supplemental information can be found online at https://doi.org/10.1016/j.xgen.2022.100163.

ACKNOWLEDGMENTS

We thank Vittore Scolari for discussion and advice on the contact analysis of the flocculin genes. We thank Laura McCulloch and Vittore Scolari for their comments on the manuscript. This work was supported in part by National Science Foundation grants MCB-1616111 and MCB-1921641 to J.D.B. L.L.-S. was supported in part by a fellowship from the Fondation pour la Recherche Médicale. This research was supported by funding to R.K. from the European Research Council under the Horizon 2020 Program (ERC grant agreement 771813).

AUTHOR CONTRIBUTIONS

L.L.-S., R.K., and J.D.B. designed the research. L.L.-S., A.T., and J.L. performed the experiments. L.L.-S., R.M., and X.S. analyzed the data, with contributions from A.T. J.M. generated the 3D representations. L.L.-S., R.K., and J.D.B. wrote the manuscript.

DECLARATION OF INTERESTS

J.D.B. is a founder and director of CDI Labs, a founder of Neochromosome, Inc, a founder of and consultant to Re-Open Diagnostics, and serves or served on the Scientific Advisory Boards of Modern Meadow, Rome Therapeutics, Sample6, Sangamo, Tessera Therapeutics, and the Wyss Institute. The remaining authors declare no competing interests.

Received: August 30, 2021
Revised: March 30, 2022
Accepted: July 6, 2022
Published: July 27, 2022

REFERENCES

1. Goffeau, A., Barrell, B.G., Bussey, H., Davis, R.W., Dujon, B., Feldmann, H., Galibert, F., Hoheisel, J.D., Jacq, C., Johnston, M., et al. (1996). Life with 6000 genes. Science *274*, 546–563-7.
2. Gregory, T.R., Nicol, J.A., Tamm, H., Kullman, B., Kullman, K., Leitch, I.J., Murray, B.G., Kapraun, D.F., Greilhuber, J., and Bennett, M.D. (2007). Eukaryotic genome size databases. Nucleic Acids Res. *35*, D332–D338.
3. Gregory, T.R. (2001). Coincidence, coevolution, or causation? DNA content, cellsize, and the C-value enigma. Biol. Rev. Camb. Philos. Soc. *76*, 65–101.
4. Taddei, A., and Gasser, S.M. (2012). Structure and function in the budding yeast nucleus. Genetics *192*, 107–129.
5. Brickner, D.G., Sood, V., Tutucci, E., Coukos, R., Viets, K., Singer, R.H., and Brickner, J.H. (2016). Subnuclear positioning and interchromosomal clustering of the GAL1-10 locus are controlled by separable, interdependent mechanisms. Mol. Biol. Cell *27*, 2980–2993.
6. Taddei, A., Van Houwe, G., Nagai, S., Erb, I., van Nimwegen, E., and Gasser, S.M. (2009). The functional importance of telomere clustering: global changes in gene expression result from SIR factor dispersion. Genome Res. *19*, 611–625.
7. Hsieh, T.-H.S., Fudenberg, G., Goloborodko, A., and Rando, O.J. (2016). Micro-C XL: assaying chromosome conformation from the nucleosome to the entire genome. Nat. Methods *13*, 1009–1011.
8. Ohno, M., Ando, T., Priest, D.G., Kumar, V., Yoshida, Y., and Taniguchi, Y. (2019). Sub-nucleosomal genome structure reveals distinct nucleosome folding motifs. Cell *176*, 520–534.e25.
9. Dauban, L., Montagne, R., Thierry, A., Lazar-Stefanita, L., Bastié, N., Gadal, O., Cournac, A., Koszul, R., and Beckouët, F. (2020). Regulation of cohesin-mediated chromosome folding by Eco1 and other partners. Mol. Cell *77*, 1279–1293.e4.
10. Garcia-Luis, J., Lazar-Stefanita, L., Gutierrez-Escribano, P., Thierry, A., Cournac, A., García, A., González, S., Sánchez, M., Jarmuz, A., Montoya, A., et al. (2019). FACT mediates cohesin function on chromatin. Nat. Struct. Mol. Biol. *26*, 970–979.
11. Lazar-Stefanita, L., Scolari, V.F., Mercy, G., Muller, H., Guérin, T.M., Thierry, A., Mozziconacci, J., and Koszul, R. (2017). Cohesins and condensins orchestrate the 4D dynamics of yeast chromosomes during the cell cycle. EMBO J. *36*, 2684–2697.
12. Schalbetter, S.A., Goloborodko, A., Fudenberg, G., Belton, J.-M., Miles, C., Yu, M., Dekker, J., Mirny, L., and Baxter, J. (2017). SMC complexes differentially compact mitotic chromosomes according to genomic context. Nat. Cell Biol. *19*, 1071–1080.
13. Naumova, N., Imakaev, M., Fudenberg, G., Zhan, Y., Lajoie, B.R., Mirny, L.A., and Dekker, J. (2013). Organization of the mitotic chromosome. Science *342*, 948–953.
14. Dixon, J.R., Selvaraj, S., Yue, F., Kim, A., Li, Y., Shen, Y., Hu, M., Liu, J.S., and Ren, B. (2012). Topological domains in mammalian genomes identified by analysis of chromatin interactions. Nature *485*, 376–380.
15. Haarhuis, J.H.I., van der Weide, R.H., Blomen, V.A., Yáñez-Cuna, J.O., Amendola, M., van Ruiten, M.S., Krijger, P.H.L., Teunissen, H., Medema, R.H., van Steensel, B., et al. (2017). The cohesin Release factor WAPL Restricts chromatin loop extension. Cell *169*, 693–707.e14.
16. Nora, E.P., Lajoie, B.R., Schulz, E.G., Giorgetti, L., Okamoto, I., Servant, N., Piolot, T., van Berkum, N.L., Meisig, J., Sedat, J., et al. (2012). Spatial partitioning of the regulatory landscape of the X-inactivation centre. Nature *485*, 381–385.
17. Wutz, G., Várnai, C., Nagasaka, K., Cisneros, D.A., Stocsits, R.R., Tang, W., Schoenfelder, S., Jessberger, G., Muhar, M., Hossain, M.J., et al. (2017). Topologically associating domains and chromatin loops depend on cohesin and are regulated by CTCF, WAPL, and PDS5 proteins. EMBO J. *36*, 3573–3599.
18. Luo, J., Sun, X., Cormack, B.P., and Boeke, J.D. (2018). Karyotype engineering by chromosome fusion leads to reproductive isolation in yeast. Nature *560*, 392–396.
19. Shao, Y., Lu, N., Wu, Z., Cai, C., Wang, S., Zhang, L.-L., Zhou, F., Xiao, S., Liu, L., Zeng, X., et al. (2018). Creating a functional single-chromosome yeast. Nature *560*, 331–335.
20. Di Stefano, M., Di Giovanni, F., Pozharskaia, V., Gomar-Alba, M., Baù, D., Carey, L.B., Marti-Renom, M.A., and Mendoza, M. (2020). Impact of chromosome fusions on 3D genome organization and gene expression in budding yeast. Genetics *214*, 651–667.
21. Lazar-Stefanita, L., Scolari, V.F., Mercy, G., Muller, H., Guérin, T.M., Thierry, A., Mozziconacci, J., and Koszul, R. (2017). Cohesins and condensins orchestrate the 4D dynamics of yeast chromosomes during the cell cycle. EMBO J. *36*, 2684–2697.
22. Duan, Z., Andronescu, M., Schutz, K., McIlwain, S., Kim, Y.J., Lee, C., Shendure, J., Fields, S., Blau, C.A., and Noble, W.S. (2010). A three-dimensional model of the yeast genome. Nature *465*, 363–367.
23. Lieberman-Aiden, E., van Berkum, N.L., Williams, L., Imakaev, M., Ragoczy, T., Telling, A., Amit, I., Lajoie, B.R., Sabo, P.J., Dorschner, M.O., et al. (2009). Comprehensive mapping of long-range interactions reveals folding principles of the human genome. Science *326*, 289–293.
24. Gassler, J., Brandão, H.B., Imakaev, M., Flyamer, I.M., Ladstätter, S., Bickmore, W.A., Peters, J.-M., Mirny, L.A., and Tachibana, K. (2017). A mechanism of cohesin-dependent loop extrusion organizes zygotic genome architecture. EMBO J. *36*, 3600–3618.
25. de Gennes, P.G. (1980). Conformations of polymers attached to an interface. Macromolecules *13*, 1069–1075.
26. Tjong, H., Gong, K., Chen, L., and Alber, F. (2012). Physical tethering and volume exclusion determine higher-order genome organization in budding yeast. Genome Res. *22*, 1295–1305.
27. Wong, H., Marie-Nelly, H., Herbert, S., Carrivain, P., Blanc, H., Koszul, R., Fabre, E., and Zimmer, C. (2012). A predictive computational model of the dynamic 3D interphase yeast nucleus. Curr. Biol. *22*, 1881–1890.
28. Zhao, B., and Brittain, W.J. (2000). Polymer brushes: surface-immobilized macromolecules. Prog. Polym. Sci. *25*, 677–710.
29. Miele, A., Bystricky, K., and Dekker, J. (2009). Yeast silent mating type loci form heterochromatic clusters through silencer protein-dependent long-range interactions. PLoS Genet. *5*, e1000478.
30. Luo, J., Mercy, G., Vale-Silva, L.A., Sun, X., Agmon, N., Zhang, W., Yang, K., Stracquadanio, G., Thierry, A., Ahn, J.Y., et al. (2018). Synthetic chromosome fusion: effects on genome structure and function. Preprint at bioRxiv. https://doi.org/10.1101/381137.

31. Sampermans, S., Mortier, J., and Soares, E.V. (2005). Flocculation onset in Saccharomyces cerevisiae: the role of nutrients. J. Appl. Microbiol. *98*, 525–531.

32. Teunissen, A.W., and Steensma, H.Y. (1995). Review: the dominant flocculation genes of Saccharomyces cerevisiae constitute a new subtelomeric gene family. Yeast *11*, 1001–1013.

33. Ogata, T., Izumikawa, M., Kohno, K., and Shibata, K. (2008). Chromosomal location of Lg-FLO1 in bottom-fermenting yeast and the FLO5 locus of industrial yeast. J. Appl. Microbiol. *105*, 1186–1198.

34. Verstrepen, K.J., Jansen, A., Lewitter, F., and Fink, G.R. (2005). Intragenic tandem repeats generate functional variability. Nat. Genet. *37*, 986–990.

35. Halme, A., Bumgarner, S., Styles, C., and Fink, G.R. (2004). Genetic and epigenetic regulation of the FLO gene family generates cell-surface variation in yeast. Cell *116*, 405–415.

36. Nieduszynski, C.A., Hiraga, S.i., Ak, P., Benham, C.J., and Donaldson, A.D. (2007). OriDB: a DNA replication origin database. Nucleic Acids Res. *35*, D40–D46.

37. Fang, D., Lengronne, A., Shi, D., Forey, R., Skrzypczak, M., Ginalski, K., Yan, C., Wang, X., Cao, Q., Pasero, P., and Lou, H. (2017). Dbf4 recruitment by forkhead transcription factors defines an upstream rate-limiting step in determining origin firing timing. Genes Dev. *31*, 2405–2415.

38. Natsume, T., Müller, C.A., Katou, Y., Retkute, R., Gierliński, M., Araki, H., Blow, J.J., Shirahige, K., Nieduszynski, C.A., and Tanaka, T.U. (2013). Kinetochores coordinate pericentromeric cohesion and early DNA replication by Cdc7-Dbf4 kinase recruitment. Mol. Cell *50*, 661–674.

39. Pohl, T.J., Brewer, B.J., and Raghuraman, M.K. (2012). Functional centromeres determine the activation time of pericentric origins of DNA replication in Saccharomyces cerevisiae. PLoS Genet. *8*, e1002677.

40. Müller, C.A., Hawkins, M., Retkute, R., Malla, S., Wilson, R., Blythe, M.J., Nakato, R., Komata, M., Shirahige, K., de Moura, A.P.S., and Nieduszynski, C.A. (2014). The dynamics of genome replication using deep sequencing. Nucleic Acids Res. *42*, e3.

41. Alvino, G.M., Collingwood, D., Murphy, J.M., Delrow, J., Brewer, B.J., and Raghuraman, M.K. (2007). Replication in hydroxyurea: it's a matter of time. Mol. Cell Biol. *27*, 6396–6406.

42. Yabuki, N., Terashima, H., and Kitada, K. (2002). Mapping of early firing origins on a replication profile of budding yeast. Gene Cell. *7*, 781–789.

43. D'Amours, D., Stegmeier, F., and Amon, A. (2004). Cdc14 and condensin control the dissolution of cohesin-independent chromosome linkages at Repeated DNA. Cell *117*, 455–469.

44. Guacci, V., Hogan, E., and Koshland, D. (1994). Chromosome condensation and sister chromatid pairing in budding yeast. J. Cell Biol. *125*, 517–530.

45. Guérin, T.M., Béneut, C., Barinova, N., López, V., Lazar-Stefanita, L., Deshayes, A., Thierry, A., Koszul, R., Dubrana, K., and Marcand, S. (2019). Condensin-mediated chromosome folding and internal telomeres drive dicentric severing by cytokinesis. Mol. Cell *75*, 131–144.e3.

46. Hirano, T. (2017). Capturing condensin in chromosomes. Nat. Genet. *49*, 1419–1420.

47. Petela, N.J., Gligoris, T.G., Metson, J., Lee, B.-G., Voulgaris, M., Hu, B., Kikuchi, S., Chapard, C., Chen, W., Rajendra, E., et al. (2018). Scc2 is a potent activator of cohesin's ATPase that promotes loading by binding Scc1 without Pds5. Mol. Cell *70*, 1134–1148.e7.

48. Muller, H., Scolari, V.F., Agier, N., Piazza, A., Thierry, A., Mercy, G., Descorps-Declere, S., Lazar-Stefanita, L., Espeli, O., Llorente, B., et al. (2018). Characterizing meiotic chromosomes' structure and pairing using a designer sequence optimized for Hi-C. Mol. Syst. Biol. *14*, e8293.

49. Matthey-Doret, C., Baudry, L., Breuer, A., Montagne, R., Guiglielmoni, N., Scolari, V., Jean, E., Campeas, A., Chanut, P.H., Oriol, E., et al. (2020). Computer vision for pattern detection in chromosome contact maps. Nat. Commun. *11*, 5795.

50. Scolari, V.F., Mercy, G., Koszul, R., Lesne, A., and Mozziconacci, J. (2018). Kinetic signature of cooperativity in the irreversible collapse of a polymer. Phys. Rev. Lett. *121*, 057801.

51. Maass, P.G., Barutcu, A.R., Weiner, C.L., and Rinn, J.L. (2018). Inter-chromosomal contact properties in live-cell imaging and in Hi-C. Mol. Cell *70*, 188–189.

52. Guérin, T.M., Béneut, C., Barinova, N., López, V., Lazar-Stefanita, L., Deshayes, A., Thierry, A., Koszul, R., Dubrana, K., and Marcand, S. (2019). Condensin-mediated chromosome folding and internal telomeres drive dicentric severing by cytokinesis. Mol. Cell *75*, 131–144.e3.

53. Paul, M.R., Markowitz, T.E., Hochwagen, A., and Ercan, S. (2018). Condensin depletion causes genome decompaction without altering the level of global gene expression in Saccharomyces cerevisiae. Genetics *210*, 331–344.

54. Ercan, S., Dick, L.L., and Lieb, J.D. (2009). The C. elegans dosage compensation complex propagates dynamically and independently of X chromosome sequence. Curr. Biol. *19*, 1777–1787.

55. McCarroll, R.M., and Fangman, W.L. (1988). Time of replication of yeast centromeres and telomeres. Cell *54*, 505–513.

56. Raghuraman, M.K., Winzeler, E.A., Collingwood, D., Hunt, S., Wodicka, L., Conway, A., Lockhart, D.J., Davis, R.W., Brewer, B.J., and Fangman, W.L. (2001). Replication dynamics of the yeast genome. Science *294*, 115–121.

57. Verstrepen, K.J., and Klis, F.M. (2006). Flocculation, adhesion and biofilm formation in yeasts. Mol. Microbiol. *60*, 5–15.

58. Liu, H., Styles, C.A., and Fink, G.R. (1996). Saccharomyces cerevisiae S288c has a mutation in Flo8, a gene required for filamentous growth. Genetics *144*, 967–978.

59. Schneider, C.A., Rasband, W.S., and Eliceiri, K.W. (2012). NIH Image to ImageJ: 25 years of image analysis. Nat. Methods *9*, 671–675.

60. Hartwell, L.H., Mortimer, R.K., Culotti, J., and Culotti, M. (1973). Genetic control of the cell division cycle in yeast: V. Genetic analysis of cdc mutants. Genetics *74*, 267–286.

61. Belton, J.-M., McCord, R.P., Gibcus, J.H., Naumova, N., Zhan, Y., and Dekker, J. (2012). Hi–C: a comprehensive technique to capture the conformation of genomes. Methods *58*, 268–276.

62. Imakaev, M., Fudenberg, G., McCord, R.P., Naumova, N., Goloborodko, A., Lajoie, B.R., Dekker, J., and Mirny, L.A. (2012). Iterative correction of Hi-C data reveals hallmarks of chromosome organization. Nat. Methods *9*, 999–1003.

63. Langmead, B., and Salzberg, S.L. (2012). Fast gapped-read alignment with Bowtie 2. Nat. Methods *9*, 357–359.

64. Cournac, A., Marie-Nelly, H., Marbouty, M., Koszul, R., and Mozziconacci, J. (2012). Normalization of a chromosomal contact map. BMC Genom. *13*, 436.

65. Lesne, A., Riposo, J., Roger, P., Cournac, A., and Mozziconacci, J. (2014). 3D genome reconstruction from chromosomal contacts. Nat. Methods *11*, 1141–1143.

66. Morlot, J.-B., Mozziconacci, J., and Lesne, A. (2016). Network concepts for analyzing 3D genome structure from chromosomal contact maps. EPJ Nonlinear Biomed. Phys. *4*, 2–15.

67. Sammon, J.W. (1969). A nonlinear mapping for data structure analysis. IEEE Trans. Comput. *C-18*, 401–409.

68. Dobin, A., Davis, C.A., Schlesinger, F., Drenkow, J., Zaleski, C., Jha, S., Batut, P., Chaisson, M., and Gingeras, T.R. (2013). STAR: ultrafast universal RNA-seq aligner. Bioinformatics *29*, 15–21.

69. Love, M.I., Huber, W., and Anders, S. (2014). Moderated estimation of fold change and dispersion for RNA-seq data with DESeq2. Genome Biol. *15*, 550.

70. Proux-Wéra, E., Armisén, D., Byrne, K.P., and Wolfe, K.H. (2012). A pipeline for automated annotation of yeast genome sequences by a conserved-synteny approach. BMC Bioinformatics *13*, 237.

STAR METHODS

KEY RESOURCES TABLE

REAGENT or RESOURCE	SOURCE	IDENTIFIER
Chemicals, peptides, and recombinant proteins		
Certified Megabase Agarose	BioRad	Cat#161-3108
SYTOX green	Thermo Fischer	Cat# S7020
Alpha-Factor	Zymo Research	Cat#Y1001
RNAse A, DNase and protease-free	Thermo Fischer	Cat#EN0531
Concanavalin a from *Canavalia ensiformis* (Jack bean),Type VI, lyophilized powder	Sigma-Aldrich	Cat#L7647-250MG
Formaldehyde 37%	Sigma-Aldrich	Cat#F8775-4X25ML
Nocodazole	Sigma-Aldrich	Cat#M1404
DpnII	NEB	Cat#R0543M
Biotin-14-dCTP	Invitrogen	Cat#19518018
DNA Polymerase I Klenow Fragment	NEB	Cat#M0210L
T4 DNA ligase	Thermo Fischer	Cat#EL0014
Proteinase K	Thermo Scientific	Cat#EO0492
T4 DNA Polymerase	NEB	Cat#M0203L
Dynabeads MyOne Streptavidin C1	Invitrogen	Cat#65001
Hydroxyurea,98%, powder	Sigma-Aldrich	Cat# H8627-25G
Glass beads, acid-washed	Sigma-Aldrich	Cat#G8772-100G
Critical commercial assays		
DNA size markers *S. pombe* chromosomal DNA	BioRad	Cat#170-3633
VK05 Lysing KIT	Ozyme	Cat#0042
NEBNext Ultra II FS kit	NEB	Cat#E7805L
Nextseq 500/550 High Output Kit v2.5 (150 Cycles)	Illumina	Cat# 20024907
NextSeq High-output 75-cycle V2.5 Kit	Illumina	Cat#20024906
Deposited data		
Raw microscopy images	This study; Mendeley	https://data.mendeley.com/datasets/swdfkxzzk7/1
Raw FASQ files	This study	BioProject: PRJNA757122 https://www.ncbi.nlm.nih.gov/bioproject/PRJNA757122 Submission ID: SUB10236799
Experimental models: Organisms/strains		
S. cerevisiae. Genotype: *MAT***a** *his3Δ1 leu2Δ0 met15Δ0 ura3Δ0;* chromosome# n = 16	Brachmann et al., 1998	BY4741
S. cerevisiae. Genotype: *MAT***a** *his3Δ1 leu2Δ0 met15Δ0 ura3Δ0;* chromosome# n = 3	Luo et al., 2018	JL381
S. cerevisiae. Genotype: *MAT***a** *his3Δ1 leu2Δ0 met15Δ0 ura3Δ0;* chromosome# n = 3	Luo et al., 2018	JL410
S. cerevisiae. Genotype: *MAT***a** *his3Δ1 leu2Δ0 met15Δ0 ura3Δ0;* chromosome# n = 2 size-matched size	Luo et al., 2018	JL402
S. cerevisiae. Genotype: *MAT***a** *his3Δ1 leu2Δ0 met15Δ0 ura3Δ0;* chromosome# n = 2 unmatched size	This study	JL498
S. cerevisiae. Genotype: *MAT***a** *his3Δ1 leu2Δ0 met15Δ0 ura3Δ0 cdc15-2(ts);* chromosome# n = 3	This study	LS381
S. cerevisiae. Genotype: *MAT***a** *his3Δ1 leu2Δ0 met15Δ0 ura3Δ0 cdc15-2(ts);* chromosome# n = 2 size-matched size	This study	LS402

(*Continued on next page*)

Continued		
REAGENT or RESOURCE	SOURCE	IDENTIFIER
S. cerevisiae. Genotype: *MAT***a** *his3Δ1 leu2Δ0 met15Δ0 ura3Δ0 NUP49::mScarlet-S.p.HIS5;* chromosome# n = 16	This study	LS125
S. cerevisiae. Genotype: *MAT***a** *his3Δ1 leu2Δ0 met15Δ0 ura3Δ0 NUP49::mScarlet-S.p.HIS5;* chromosome# n = 2 size-matched size	This study	LS126
Oligonucleotides		
chr11R-gRNA for CRISPR-Cas9 AAATGAAGAAGTGCCATGGG	This study	n/a
chr5L-gRNA for CRISPR-Cas9 TTTCACATGCTCGACCGTTT	This study	n/a
cen7-gRNA TATTTTATTGTCGGTGTTTG	This study	n/a
Recombinant DNA		
Plasmid: TEF1p-CRISPR-Cas9	Luo et al., 2018	
Software and algorithms		
ImageJ	Schneider et al., 2012	https://imagej.nih.gov/ij/
Matlab 2018	MATLAB 2018a, The MathWorks, Inc., Natick, Massachusetts, United States.	https://www.mathworks.com/products/matlab.html mat2pdb: https://fr.mathworks.com/matlabcentral/fileexchange/42957-read-and-write-pdb-files-using-matlab
FlowJo v10.0.7	Becton, Dickinson and Company; 2021	https://www.flowjo.com/
Bowtie 2	Langmead and Salzberg, 2012	http://bowtie-bio.sourceforge.net/bowtie2/index.shtml
Clustal Omega	Sievers et al., 2011	https://www.ebi.ac.uk/Tools/msa/clustalo/
PyMOL	Molecular Graphics System, Version 2.0 Schrödinger, LLC	https://pymol.org/edu/
DEseq2	Love et al., 2014	https://bioconductor.org/packages/release/bioc/html/DESeq2.html
Other		
Saccharomyces Genome Database | SGD for S288c reference genome files		https://www.yeastgenome.org/
Yeast genome annotation pipeline - YGAP	Proux-Wera et al., 2012	http://wolfe.ucd.ie/annotation/index.html#questioncheck1

RESOURCE AVAILABILITY

Lead contact

Further information and requests for resources should be directed to Jef D. Boeke (jef.boeke@nyulangone.org).

Materials availability

Yeast strains generated in this study can be requested directly by contacting the lead contact.
This study did not generate new unique reagents.

Data and code availability

Raw microscopy images were deposited on Mendeley at: https://data.mendeley.com/datasets/swdfkxzzk7/1.
FASTQ files of GWS (HiC datasets and RNA sequencing) in were deposited in the NCBI GEO database.
BioProject: PRJNA757122 https://www.ncbi.nlm.nih.gov/bioproject/PRJNA757122.
Submission ID: SUB10236799.
No new code was generated in this study.

EXPERIMENTAL MODEL AND SUBJECT DETAILS

Yeast strains used in this work are listed in STAR Methods - Key resources table. JL498 was generated using a CRISPR-Cas9 method from a parent that was generated in a previous study JL410.[18] This involved fusing the right arm of chromosome 14 to the left arm of chromosome 5 and deleting *CEN7* using a combination of three gRNAs: chr14R-gRNA, chr5L-gRNA and cen7-gRNA (refer to the oligonucleotides section in the Key resources table).

METHOD DETAILS

Media and culture conditions

All strains were grown in rich medium (YPD: 1% bacto peptone (Difco), 1% bacto yeast extract (Difco) and 2% glucose). Cells were grown at either 30°C or 23–25°C (the latter temperature corresponding to the permissive temperature of *cdc15-2*; see below).

Spot assays

Spot assays were performed as previously described by Luo et al.[18] except that the culture was initially diluted to A_{600} = 0.1.

Pulsed-field gel electrophoresis

Pulsed-field gel electrophoresis (PFGE) was carried out as we previously described,[18] with running conditions recommended for *S. pombe* chromosomes (BioRad No.170-3633) to achieve separation of the large fused chromosomes.

DNA staining

Approximately 10^7 cells/sample were fixed in 70% ethanol and stored at 4°C overnight. Cell pellets were washed twice with RNAse solution (10 mM Tris pH 8.0, 15 mM NaCl) and treated with 0.1 mg/mL RNAse A for 3–4 h at 37°C. Cells were centrifuged, washed once with 50 mM Tris pH 7.5 and resuspended in labeling solution (1 μM SYTOX Green in 50 mM Tris pH 7.5; ThermoFisher) for 1 h at 4°C. Before imaging and flow cytometry data acquisition, cells were washed twice and resuspended in 50 mM Tris pH 7.5.

Imaging DNA occupancy and nuclear size

Estimating DNA occupancy. To minimize the variability introduced by experimental procedure, the surface area occupied by DNA was calculated in groups of samples manipulated simultaneously (on the same day). Exponentially-growing cultures were treated for DNA staining (see above). For Z-stack acquisition, concanavalin A (Sigma-Alderich) coated glass slides were used to immobilize cells. Imaging was performed using the total internal reflection fluorescence (TIRF) microscope (objective: Plan Apo VC 100× Oil DIC N2; camera: Andor Zyla VSC-03679). NIS element AR software was used for image acquisition: 470 nm excitation wavelength (3% power), 10 ms exposure time, z stack 1.8 μm range (relative positions in Z −0.9 to +0.9 μm, 7 steps of 0.3 μm). Images were imported and analyzed with ImageJ software.[59] The surface area occupied by the DNA was estimated using the "3D object counter" option after image segmentation and thresholding set at 3500-pixel intensity. Approximately 800–1500 DNA surfaces/strain (Table S4) were plotted using the violin function and the p-values were calculated using the Kolmogorov–Smirnov test (K–S test) functions available in Matlab R2018.

The increase in DNA occupancy in the size-matched n = 2 strain was correlated with an enlargement of the nuclear size in this strain compared to the wild type, n = 16. The surface area of the nucleus was measured in n = 2 (LS126) and n = 16 (LS125) yeasts, in which the nuclear envelope protein, Nup49, was tagged with mScarlet. Live cells in exponential growing phase were imaged using the EVOS M7000 microscope (Olympus X-APO 100X Oil, 1.45NA/WD 0.13mm oil objective). Images were analyzed with ImageJ software.[59] Spherical nuclei (~150 for n = 16; ~300 for n = 2) were manually selected and, their circumference and surface area were estimated Table S5. Experiments were performed on two and three independent clones of LS125 and LS126.

Cell cycle progression

G1 arrested cells were obtained by incubating exponentially-growing cultures (~10^8 cells) with 37 μM α-factor (Zymo Research) for 150 min at 23°C. An aliquot of ~1.5 × 10^7 cells G1 cells was fixed in 70% ethanol while the remaining culture was centrifuged and washed twice with fresh medium. Pelleted cells were resuspended in fresh medium and incubated at room temperature. G1-released cultures were sampled at multiple time points throughout the entire S-to-M cell cycle progression. The corresponding aliquots were treated for DNA staining (see above). Flow cytometry was performed on a BD Accuri C6 Flow Cytometer (BD CSampler Software) and data were analyzed using FlowJo v10.0.7 software.

Cell synchronization

G1 elutriation. G1 daughter cells were recovered from exponentially-growing cultures through elutriation - a physical method of cell cycle synchronization, used to separate cells according to their density and sedimentation velocity. For a detailed protocol see Lazar-Stefanita et al.[21] After elutriation, ~1.5 × 10^9 G1 cells were suspended in 150 mL fresh YPD at 30°C for 30 min and then crosslinked with 3% formaldehyde (Sigma-Aldrich) for Hi-C library preparation (see below).

Nocodazole. Metaphase cells were chemically synchronized using the microtubule disrupting drug, nocodazole (Sigma-Aldrich). Exponentially-growing cultures (7 × 10^6 cells/mL) were grown for 3 h at 30°C in YPD supplemented with 15 μg/mL nocodazole. Cells were then crosslinked with 3% formaldehyde (Sigma-Aldrich) for Hi-C library preparation.

M phase ts mutants. Anaphase-synchronized cells were obtained through the thermosensitive (*ts*) mutant, *cdc15-2*.[60] Exponentially-growing cultures (~7 × 10^6 cells/mL) of strains, carrying the mutated *cdc15-2* allele, were transferred from the permissive temperature (25°C) to the non-permissive growing temperature (37°C). Cultures were incubated for 3 h at 37°C before being crosslinked with 3% formaldehyde (Sigma-Aldrich) for Hi-C library preparation (see below).

Hi-C: Library preparation

Hi-C experiments (Table S6) were performed following the protocol described by Belton et al.[61] For each library preparation 1–3 × 10^9 cells in 150 mL culture medium were first fixed for 20 min in 3% formaldehyde (Sigma-Aldrich), then quenched with 0.4 M glycine for other 20 min at room temperature. Cells were harvested, washed with culture medium and resuspended in chilled TE buffer supplemented with protease inhibitors. The VK05 Lysing KIT (Ozyme) at 6700 rpm was adopted to break down yeast cell wall. Lysates containing 0.5% SDS were incubated for 20 min at 65°C then digested overnight at 37°C with DpnII (final concentration 500 U/pellet; NEB). Digestion pellets were resuspended in cold water and the 5′ DpnII overhangs were filled in using a biotin-labeled 30 μM dNTP mix (dATP, dGTP, dTTP and Biotin-14-dCTP Invitrogen) and Klenow enzyme (NEB). Biotinylated DpnII restriction fragments were ligated using T4 DNA ligase (final concentration of 250 Weiss U/pellet; Thermo Fischer) for 4 h at 16°C. Cross-linking was reversed through overnight treatment in the presence of 250 μg/mL Proteinase K (Thermo Scientific) at 50°C. DNA was extracted by phenol/chloroform, precipitated and treated with 500 μg/mL RNAse A (Thermo Fischer). The effective digestion and ligation reactions were verified on agarose gel 1% (controls: non-digested and non-religated). Biotin was removed from the non-ligated DNA fragments using the T4 DNA polymerase (final concentration of 5 U/pellet; NEB). Finally, ligated fragments were sheared to a size of 500 bp using Covaris S220 and pulled down using Dynabeads MyOne Streptavidin C1 (Invitrogen). Resulting libraries were amplified by PE-PCR primers for standard paired-end deep-sequencing on NextSeq500 Illumina platform (2 × 75 bp cycles).

Hi-C: Data processing

Generating contact maps. Raw paired-end reads were processed using the HICLib algorithm,[62] adapted for the *S. cerevisiae* genome. PCR duplicates were removed before either read-pair was independently mapped using Bowtie 2[63] (mode: –very-sensitive –rdg 500,3 –rfg 500,3) on the corresponding reference sequence (S288C from SGD and fusion versions of it) indexed for DpnII restriction site. An iterative alignment with a 20 bp seed length was used to maximize the yield of uniquely mapped reads (mapping quality, MAPQ >30). The aligned reads were classified based on their assignment and orientation on the DpnII indexed reference genome. To generate contact frequency maps, the unwanted events were filtered out (e.g., loops, non-digested fragments, etc.; for details see Cournac et al.[64]) while the valid Hi-C reads were binned into units of single restriction fragment (RF). Then consecutive RFs were assigned to fixed size bins of either 5 kb or 50 kb. Bins with a high variance in contact frequency (<1.5 Standard Deviation or 1.5–2 S.D.) were discarded. To remove potential biases resulting from the uneven distribution of restriction sites and variation in GC content and mappability, filtered contact maps were normalized using the sequential component normalization procedure with L1 norm (SCN).[64] Approximately 15 million valid contacts were used to generate a genomic contact map (~400 contacts/RF; ~6500 contacts/5kb bin).

FLO contact maps. Contact enrichment maps between *FLO* genes were detected by aligning Hi-C reads on unique sequences flanking both 5′ and-3′ ends of the *FLO* coding regions. Sequence identity was verified using the multiple alignment option available for DNA in Clustal Omega on the EMBL – EBI website. Default parameters were used to align a total number of 12 10-kb long sequences upstream and downstream all *FLO* coding sequences. The alignments were used to determine the degree of % identity between all sequences (gap-exclusion identity) and to compute the "distance" between pairs (tree). Using this approach, we chose 10-kb long *FLO*-flanking sequences that display ~35% sequence identity to assemble a new reference sequence (100-kb long). Most of these DNA sequences were immediately adjacent to the coding sequence except for the 3′ UTRs of *FLO1* and *FLO5* that were placed 20 and 25 kb away, respectively. The new reference was used to generate 2D *FLO* contact maps (2kb-binned).

Contact probability on the genomic distance, p(s). Hi-C contact frequency (*p*) decreases with as genomic distance between restriction fragments increases. *p(s)* functions were computed on intrachromosomal read pairs from which self-circularizing and uncut events – identified as reads having different orientations and separated by less than 1.5 kb - were discarded. The retained reads were log-binned in function of their distance along chromosome arms, according to the following formula:

$$\text{bin} = [\log 1.1(s)]$$

Therefore, *p*(*s*) function is a histogram representation of the sum of contacts weighted by both bin-size $1.1^{(1+\text{bin})}$ and chromosome length (*s*).

Comparison of the degree of *p(s)* decay is indicative of a change in polymer state. Derivatives of the *p(s)* were computed to compare chromatin states in native versus fused chromosomes.

Contact probability was computed by "chunk," with each chunk corresponding to a 300 kb window measured as distance from the centromere (e.g., 0, 300, and 600 kb from the centromere). n = 16 and n = 2 chromosomes were divided into multiple chunks and then the intra-chunk *p(s)* decay was computed following the method described above. Finally, the average of chunk *p(s)* decay per genome was extrapolated.

Log-ratio comparison maps. To assess genome-wide contact map similarities and differences, data were first binned at 50 kb and normalized. Finally, they were compared by computing the log2 ratio between each pair.

Similarly, local contact differences at pericentromeres and SMC binding sites were computed based on 5 kb-binned contact maps.

Centromere agglomerated log ratios. Centromere positions were partitioned into centromeres retained in n = 2 (*CEN7* and *CEN15*) and deleted centromeres. For each group, in 2 kb resolution contact maps, windows surrounding the centromeres were extracted and averaged. The resulting observed signal in the n = 2 strain was divided by the signal in the n = 16 stain. The log of these ratios was then computed.

Cohesin agglomerated plots. Data from Petela et al.[47] were used to generate Scc1 ChIP-Seq profiles with a 2 kb resolution. Bins with a signal over 1.5 were labeled as cohesin binding sites (CBS). All possible pairs of CBS within chromosomal arms were determined and partitioned according to their genomic distance. In 2 kb resolution contact maps, windows surrounding these positions were extracted and averaged. The resulting observed signal was divided by the expected signal, generated by averaging windows around random positions maintaining the same genomic distance as the pairs of CBS. For each window, under-covered bins were defined as bins with a total number of reads under the median (number of reads/bin) –SD and excluded from the averaging operations to reduce noise. Eventually log2 ratio plots that display the average contact signal of all possible pairs of Scc1 enrichment sites over the average contacts of random sites in 80 kb windows were computed.

4C-like profiles. To obtain 4C-like contact profiles of a given locus, filtered-normalized contact maps at 5 kb resolutions were indexed and the selected position/s annotated. Profiles of the selected bins were extracted and plotted (log10) using Matlab 2018 (no smoothing was applied).

3D representations. For visualization purposes, Hi-C contact frequency maps can be represented as 3D structures generated using the "Shortest-path Reconstruction in 3D″ algorithm, ShRec3D.[65,66] The algorithm computes a distance matrix by inverting element-wise the corresponding 5 kb-binned contact map that was previously filtered and normalized (see Hi-C: Data processing). The resulting distance matrix is supplemented by computing shortest path distances. This procedure removes infinite values and yields values that satisfy the triangular inequality. To obtain the coordinates in 3D (x, y, z) the Sammon mapping algorithm was applied on the distance matrix.[67] Finally, the "mat2pdb" function in Matlab 2018 was used to generate pdb files, which were rendered using PyMOL (Molecular Graphics System, Version 2.0 Schrödinger, LLC). The resulting 3D structures are average representations of the contact maps and, therefore, do not represent exact structures found in individual cells. These maps must be interpreted in light of contact frequencies across large cell populations. In this work, 3D structures were not used to compare datasets; all computational analyses were performed on contact maps.

Replication timing

Each profile of replication timing was generated from three independent clones by sort-seq analysis as described previously.[40] Briefly, fractions of replicating and non-replicating cells were obtained by arresting cells in α-factor (see cell cycle progression) and then releasing them in 200 mM hydroxyurea (HU; Sigma-Aldrich) for 90 min at 30°C. Synchronization efficiency was checked by flow cytometry (see DNA staining and cell cycle progression). Pellets of ~6×10^8 cells were used to extract genomic DNA using acidic wash beads (Sigma-Aldrich) and phenol-chloroform. Library preparation was performed using the NEBNext Ultra II FS kit (NEB) according to Illumina protocol. Resulting libraries were paired-end deep-sequenced on NextSeq500 Illumina platform (2 × 36 bp cycles). Reads were mapped to the corresponding reference genome using Bowtie 2[63] in its –very-sensitive mode. Profiles of replication timing were generated by normalizing the replicating (S phase - HU) sample to the non-replicating (G1 - α-factor) sample in 1-kb bins. The resulting ratios were gaussian-smoothed and plotted by genomic coordinate. They measure relative DNA copy number as a proxy of replication time.

RNA-seq

Total RNA extraction, library preparation and sequencing followed a previously-described method[17]. Briefly, RNA-seq reads were aligned to S288C reference genome (sacCer2) using STAR with default parameters.[68] Differential expression analysis was performed using DEseq2.[69] We consider genes with log2 fold-change > 2 or < −2 and p-value < $1E10^{-5}$ to be differentially expressed (Tables S1–S3).

Genome annotation

Fused genomes were annotated using a combination of different software packages. The yeast genome annotation pipeline (YGAP)[70] online tool was used to annotate coding regions and generate general feature format (GFF) files. Other genome features (e.g., centromeres, telomeres, ARS, transposons etc.) were first mapped to the fused reference genome, and the resulting alignment files used to generate GFF3 files.

QUANTIFICATION AND STATISTICAL ANALYSIS

Information on the number of biological replicates, statistical tests and p-values is provided in the Method details and Figure legends.

Cell Genomics, Volume *2*

Supplemental information

Karyotype engineering reveals spatio-temporal control of replication firing and gene contacts

Luciana Lazar-Stefanita, Jingchuan Luo, Remi Montagne, Agnes Thierry, Xiaoji Sun, Guillaume Mercy, Julien Mozziconacci, Romain Koszul, and Jef D. Boeke

Title: Karyotype engineering reveals spatio-temporal control of replication firing and gene contacts

Authors: Luciana Lazar-Stefanita[1,2,3], Jingchuan Luo[1]†, Remi Montagne[2]†, Agnes Thierry[2], Xiaoji Sun[1], Guillaume Mercy[2], Julien Mozziconacci[4], Romain Koszul[2]*, Jef D. Boeke[1,5]*

†, These authors contributed equally

*, Corresponding authors: RK romain.koszul@pasteur.fr; JDB jef.boeke@nyulangone.org

Supplemental Figures and Tables:

Supplemental Figures 1-7, related to Main Figure 1. Nuclear organization and function of mega-sized chromosomes in *S. cerevisiae*.

Supplemental Figures 8-9, related to Main Figure 2. Contact analysis of repeat-enriched (flocculin) genes in megachromosomes.

Supplemental Figures 10-15, related to Main Figure 3. S-phase progression and DNA replication of megachromosomes.

Supplemental Figures 16-18, related to Main Figure 4. Structural reorganization of megachromosomes during cell division.

Supplemental Table 6, related to Main Figures 1, 2 and 4. Hi-C libraries.

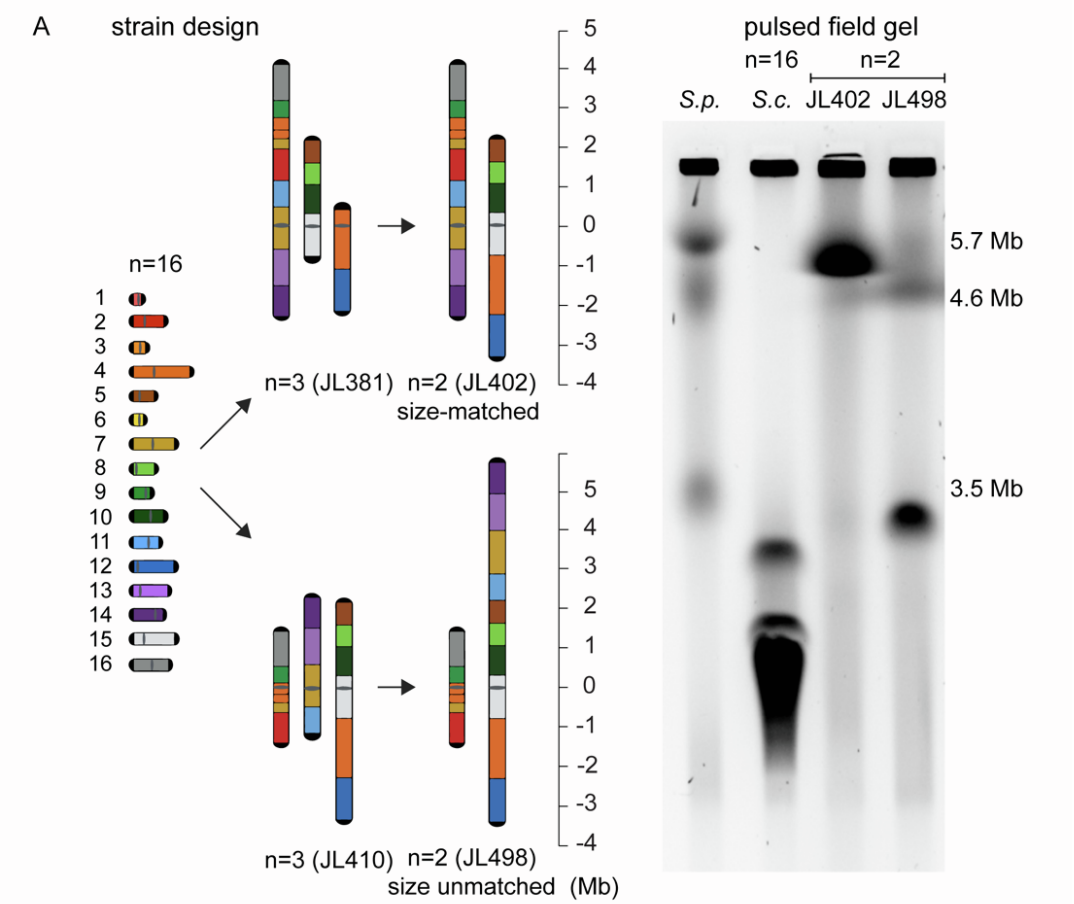
A
strain design
n=16
1
2
3
4
5
6
7
8
9
10
11
12
13
14
15
16
n=3 (JL381)
n=2 (JL402)
size-matched
n=3 (JL410)
n=2 (JL498)
size unmatched
5
4
3
2
1
0
-1
-2
-3
-4
(Mb)
pulsed field gel
n=16
n=2
S.p.
S.c.
JL402
JL498
5.7 Mb
4.6 Mb
3.5 Mb

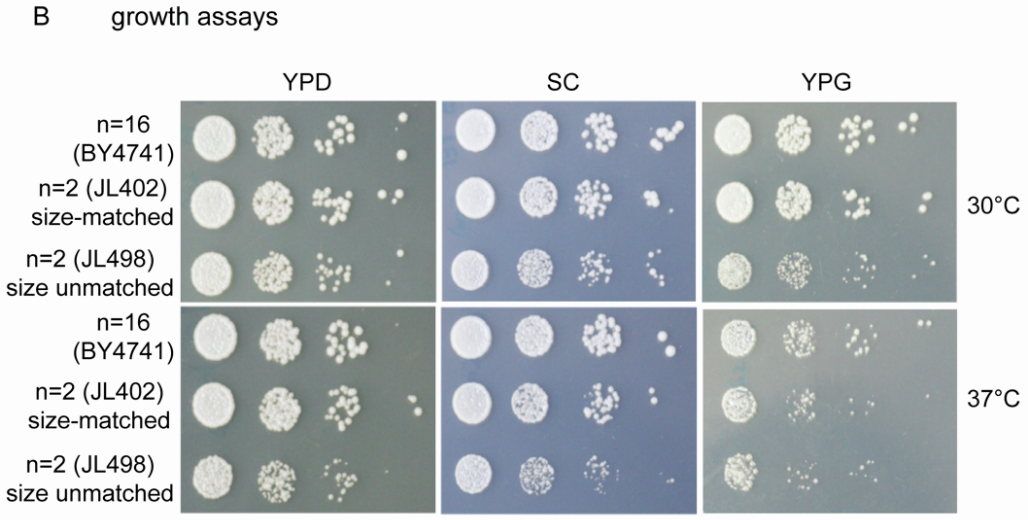
B
growth assays
YPD
SC
YPG
n=16
(BY4741)
n=2 (JL402)
size-matched
n=2 (JL498)
size unmatched
30°C
37°C

Figure S1, related to Main Figure 1. Design of size-matched and unmatched megachromosomes.

(**A**) Design of the megachromosomes. The diagram on the left illustrates the arrangement of the 16 native chromosomes into n=2 (JL402 size-matched and JL498 size unmatched) and the corresponding n=3 intermediate strains used in this study. The 16 native chromosomes are uniquely colored and ordered numerically, while the fused chromosomes are alphabetically ordered (A, B and C). Length of chromosome arms is indicated as a function of distance from the centromere position (Mb). On the right, pulsed-field gel electrophoresis with *S. pombe* (*S.p.*) chromosomal DNA as a ladder followed by *S.c.*, *S. cerevisiae*, n=2 JL402 size-matched and n=2 JL498 unmatched (for n = 3 strains refer to Luo et al.[17]). (**B**) Growth assay: serial dilutions of n=16 (BY4741) and n=2 (JL402 and JL498) on YPD (Yeast Extract–Peptone–2%Dextrose), SC (synthetic complete) and YPG (Yeast Extract–Peptone–3% Glycerol) medium at 30˚C and 37˚C.

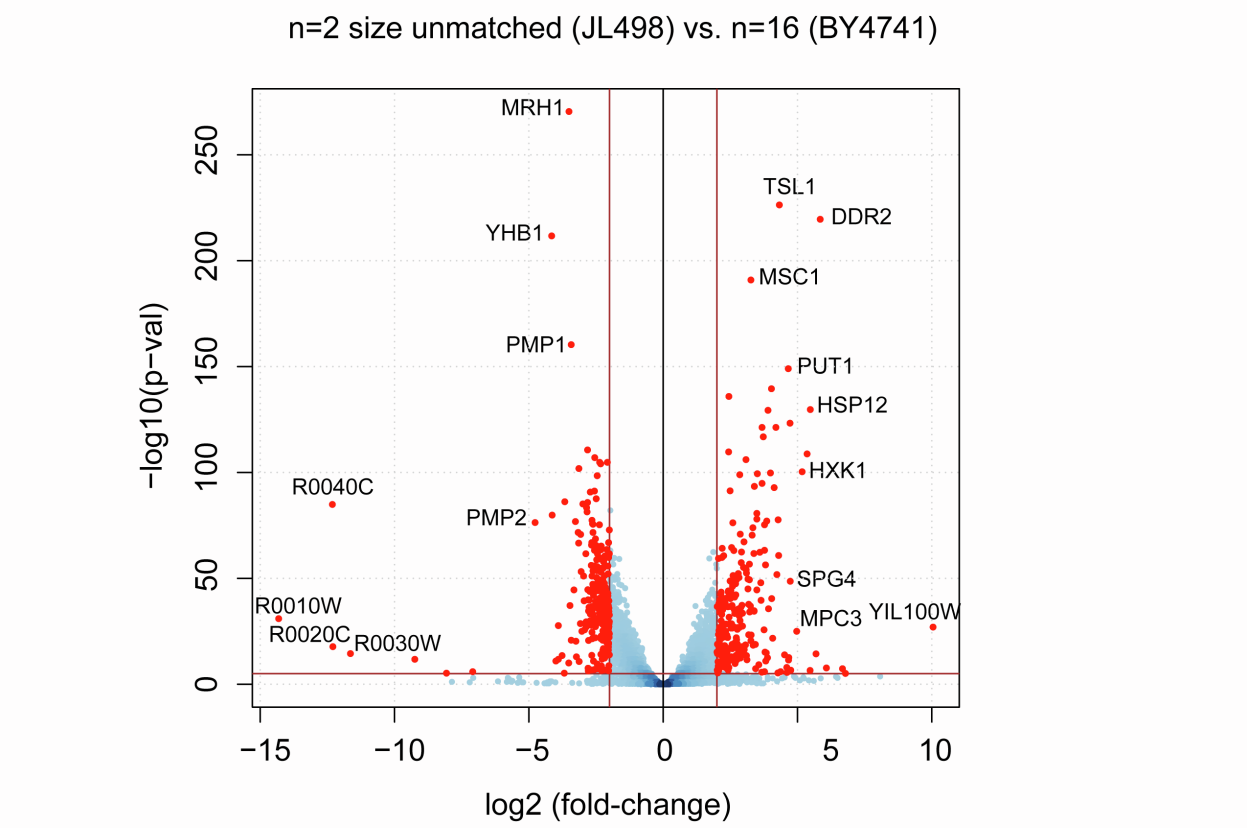

Figure S2, related to Main Figure 1. Transcriptomics of n=2 with unmatched megachromosomes.

Volcano plot of RNA-seq data that compares the transcriptomes of n=16 and n=2 JL498 (for n = 2 JL402 strain refer to Luo et al.[30]). Red dots indicate genes whose expression was significantly different in the n = 2 strain compared to the n = 16 strain (log2 fold-change > 2 or < -2 and *P*-value < $1E10^{-5}$).

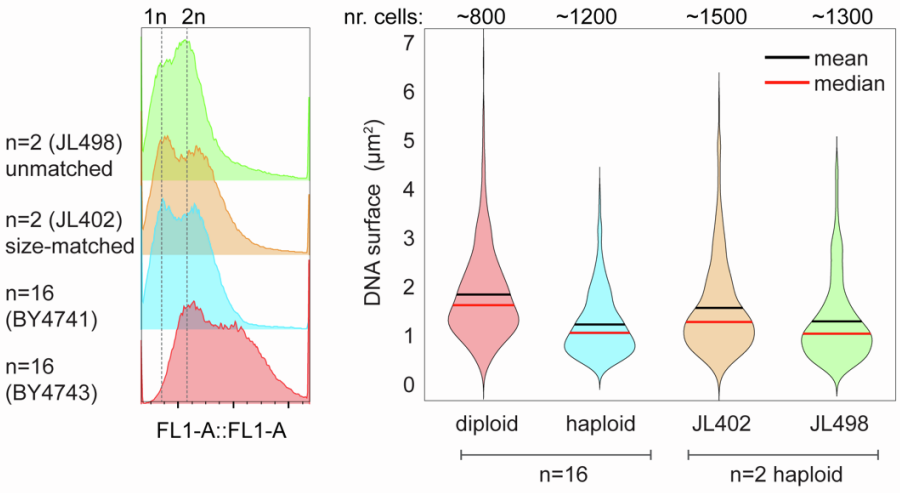

DNA surface (µm²)	n=16 haploid (BY4741)		n=16 diploid (BY4743)		n=2 size-matched haploid (JL402)			n=2 unmatched haploid (JL498)		
	R1	R2	R1	R2	R1	R2	R3	R1	R2	R3
MED (µm²)	1.11	1.15	1.68	1.68	1.34	1.46	1.46	1.10	1.27	1.17
MX (µm²)	1.28	1.35	1.90	1.99	1.62	1.69	1.73	1.35	1.56	1.43
DNA surface increase relative to n=16 (BY4741)	%		50%	47%	26%	25%	28%	0%	15%	6%
	p-val		4.36^{-28}	9.09^{-22}	2.56^{-05}	6.91^{-08}	1.27^{-13}	0.65	0.013	0.15

MED (µm²) = median MX (µm²) = mean R(n°) = independent replicates

Summary measurements Supplemental Table 2a

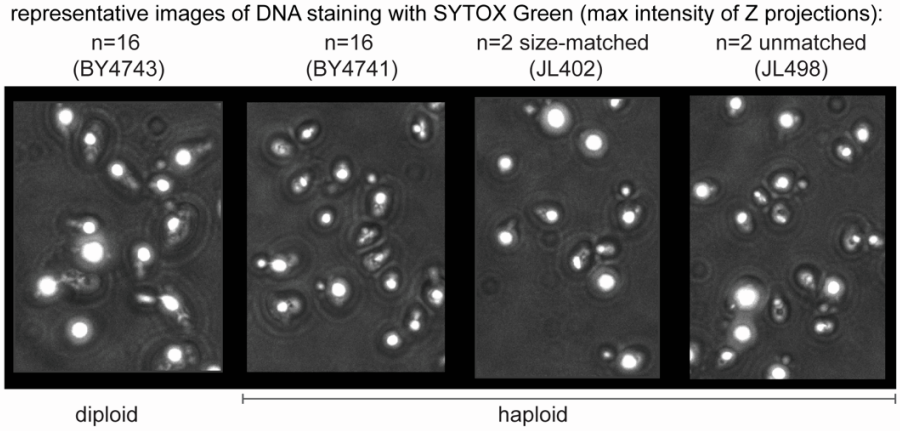

Figure S3, related to Main Figure 1. DNA content and surface in yeasts with n=2 megachromosomes.

Flow cytometry histograms of DNA content and microscopy on SYTOX Green-stained cells of n=16 (BY4743 and BY4741) and n=2 (JL402 and JL498) strains. Violin plots display mean and median values of the DNA surface (µm^2) in haploid (n=16 and n=2) and diploid (n=16 BY4743, positive control for surface increase) strains. Summary table of DNA surface (µm^2) measurements for each independent replicate (R#) showing: their relative (%) increments as compared to n=16 haploid and *P*-values obtained from K-S test. Bottom panels: representative images of GFP excited cells used above.

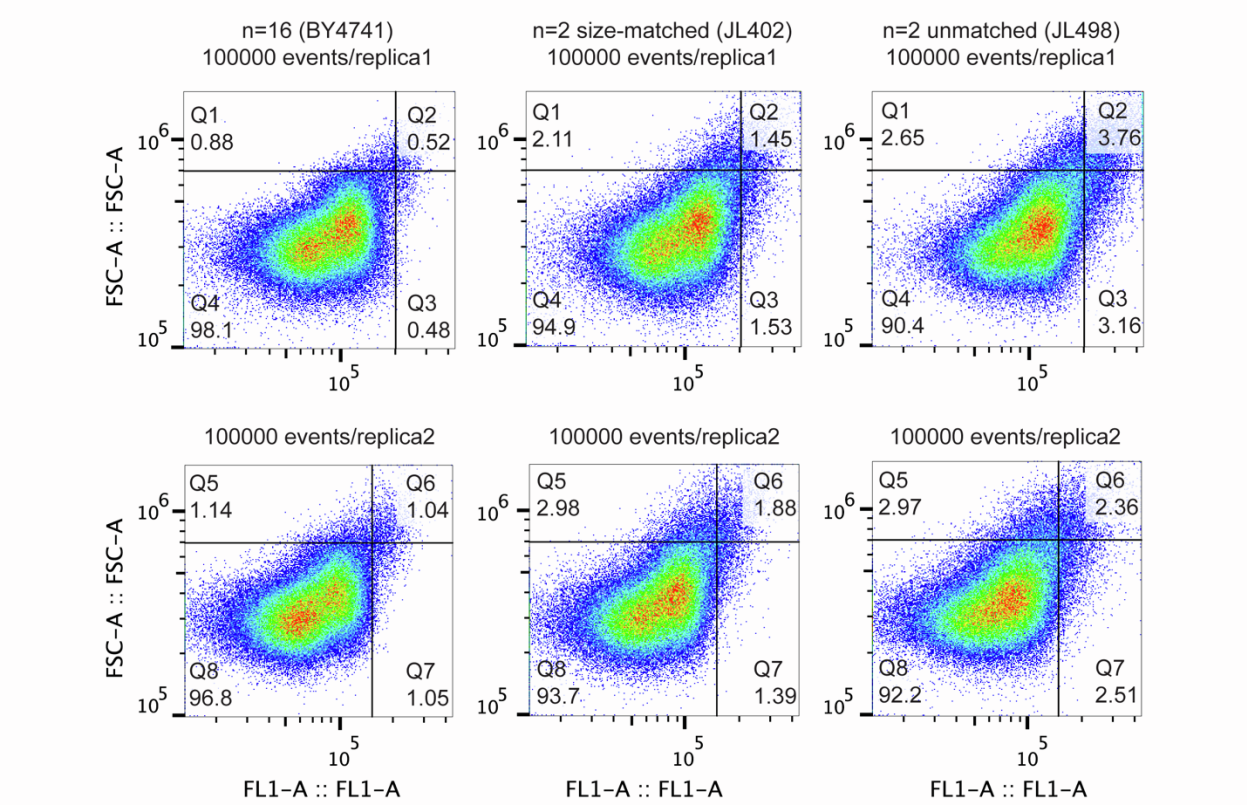

Figure S4, related to Main Figure 1. N=2 yeasts display a mild excess in DNA content. Flow cytometry of haploid cell populations (100,000 events). *x*- and *y*-axis indicate cell size (FSC) and DNA content (FL1) respectively. Note that both n=2 strains display a slight increase in number of cells with an excess of DNA content and/or size relative to n=16.

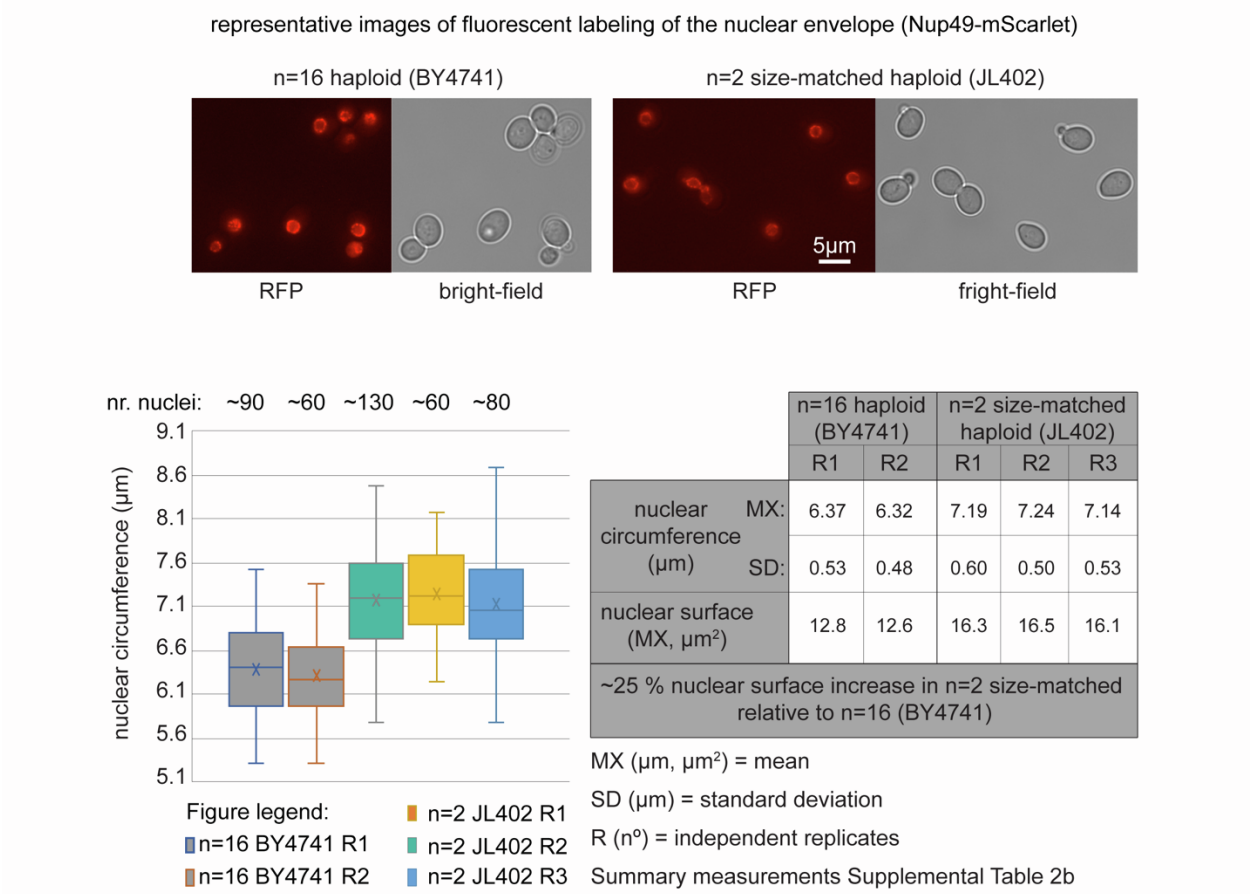

		n=16 haploid (BY4741)		n=2 size-matched haploid (JL402)		
		R1	R2	R1	R2	R3
nuclear circumference (µm)	MX:	6.37	6.32	7.19	7.24	7.14
	SD:	0.53	0.48	0.60	0.50	0.53
nuclear surface (MX, µm²)		12.8	12.6	16.3	16.5	16.1
~25 % nuclear surface increase in n=2 size-matched relative to n=16 (BY4741)						

MX (µm, µm²) = mean

SD (µm) = standard deviation

R (nº) = independent replicates

Summary measurements Supplemental Table 2b

Figure S5, related to Main Figure 1. Nuclear size increases in n=2 with size-matched megachromosomes.

Nuclear size in haploid cells of n=16 (BY4741) and n=2 size-matched (JL402) with Nup49 (nuclear pore protein) fluorescently tagged with mScarlet. Top panels: representative microscopy images. Bottom panels: mean (MX) and standard deviation (SD) of nuclear circumference (µm) and surface (µm^2).

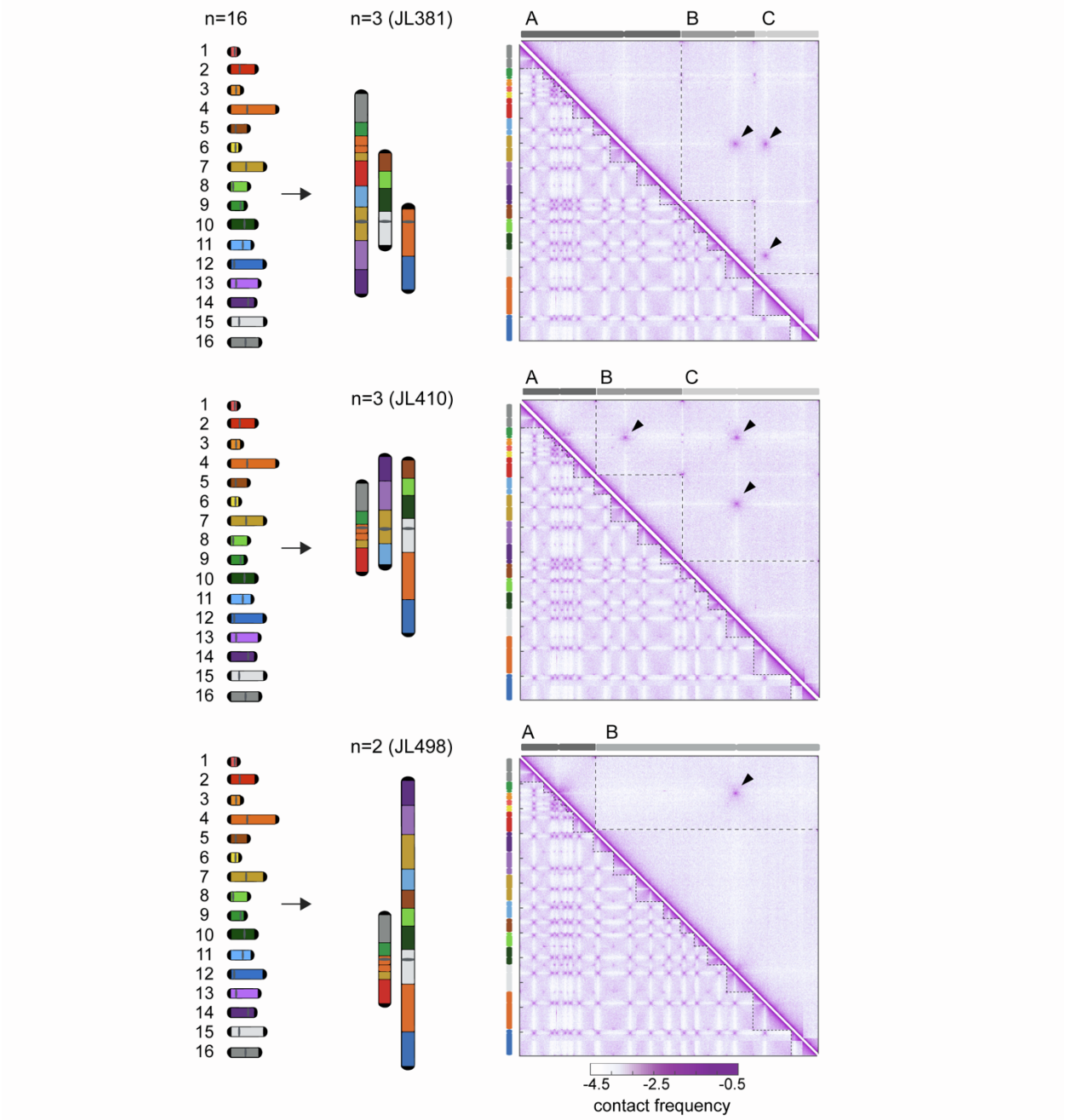

Figure S6, related to Main Figure 1. 3D organization (Hi-C) of megachromosomes.
Contact maps of n=16, n=3 and n=2 (JL498, unmatched size). Diagrams on the left illustrate the design of each fusion while panels on the right show the corresponding Hi-C contact maps. Top left maps were generated by aligning n=3 and n=2 reads to reference sequences containing either 3 or 2 megachromosomes (A, B and/or C, atop the map). Bottom left maps show all 16 native chromosomes in n=16. Chromosomes on the Hi-C maps (5 kb-binned) appear underlined by dotted lines. Black arrowheads point at inter-pericentromeric contacts. Violet to white color scale reflects high to low contact frequencies (log10).

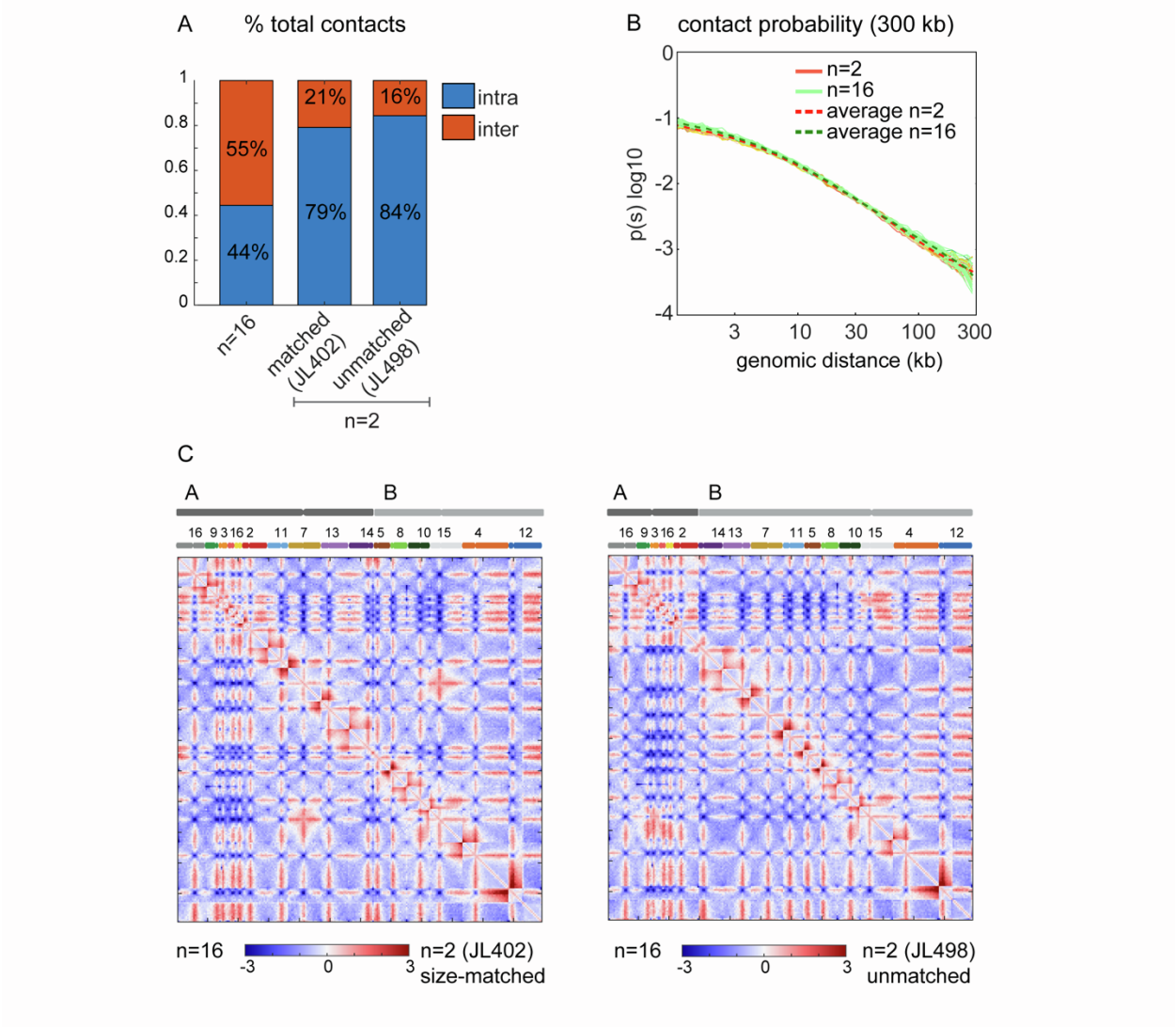

Figure S7, related to Main Figure 1. Contact analysis of megachromosomes.
(**A**) Quantitative bar chart showing the relative (%) of intra- and inter-chromosome contacts in n=16 and n=2 (JL402 and JL498). (**B**) Contact probability, *p*(*s*), spanning 300 kb genomic windows in n=16 and n=2, dash line represents the average decay of the intrachromosomal contact frequency *p* between loci with respect to their genomic distance *s*. (**C**) Log2-ratios between contact maps (50kb-binned). Left map: n=16 vs. n=2 size-matched (JL402). Right map: n=16 vs. n=2 unmatched (JL498). Blue to red color scale reflects the enrichment in contacts in n=2 with respect to n=16 (log2). Chromosomes are annotated atop the maps.

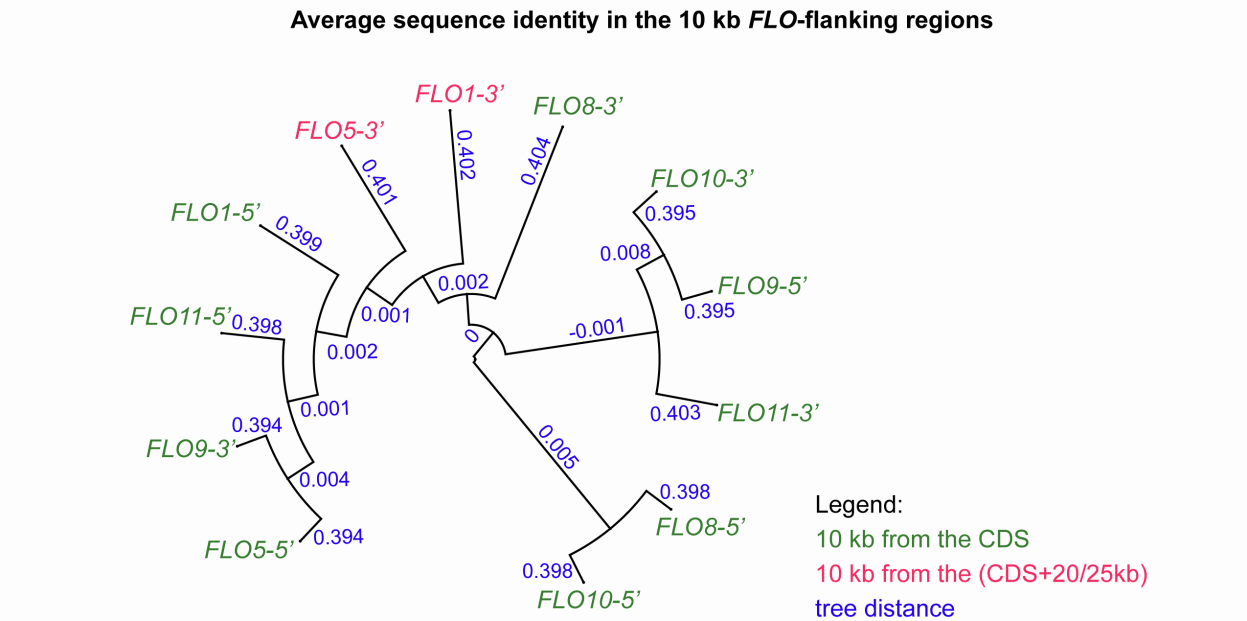

Percent Identity Matrix - created by Clustal 2.1

	FLO10-5'	FLO8-5'	FLO11-3'	FLO9-5'	FLO10-3'	FLO8-3'	FLO1-3'	FLO5-3'	FLO1-5'	FLO11-5'	FLO9-3'	FLO5-5'
FLO10-5'	**100.00**	46.05	33.18	32.64	33.35	34.26	33.02	33.12	34.78	33.57	33.59	33.72
FLO8-5'	46.05	**100.00**	32.55	33.72	33.51	33.55	32.24	33.53	35.07	34.11	34.11	34.63
FLO11-3'	33.18	32.55	**100.00**	40.21	41.78	32.70	32.99	32.95	32.65	32.36	32.32	33.29
FLO9-5'	32.64	33.72	40.21	**100.00**	45.23	32.17	32.56	32.60	32.23	32.15	33.04	32.78
FLO10-3'	33.35	33.51	41.78	45.23	**100.00**	33.45	32.54	33.48	33.45	32.91	33.61	33.74
FLO8-3'	34.26	33.55	32.70	32.17	33.45	**100.00**	37.84	36.61	37.09	36.93	37.40	37.14
FLO1-3'	33.02	32.24	32.99	32.56	32.54	37.84	**100.00**	37.70	37.45	37.98	37.91	37.86
FLO5-3'	33.12	33.53	32.95	32.60	33.48	36.61	37.70	**100.00**	38.56	37.72	38.08	38.51
FLO1-5'	34.78	35.07	32.65	32.23	33.45	37.09	37.45	38.56	**100.00**	38.77	40.17	40.16
FLO11-5'	33.57	34.11	32.36	32.15	32.91	36.93	37.98	37.72	38.77	**100.00**	40.67	41.36
FLO9-3'	33.59	34.11	32.32	33.04	33.61	37.40	37.91	38.08	40.17	40.67	**100.00**	45.81
FLO5-5'	33.72	34.63	33.29	32.78	33.74	37.14	37.86	38.51	40.16	41.36	45.81	**100.00**

Figure S8, related to Main Figure 2. Sequence identity in the flocculin flanking genes.
Tree diagram and identity matrix illustrate the relative sequence identity between all 10kb regions adjacent to the CDS (CoDing Sequence) of each *FLO* gene. A ~35% sequence identity was obtained using the multiple alignment option in Clustal Omega.

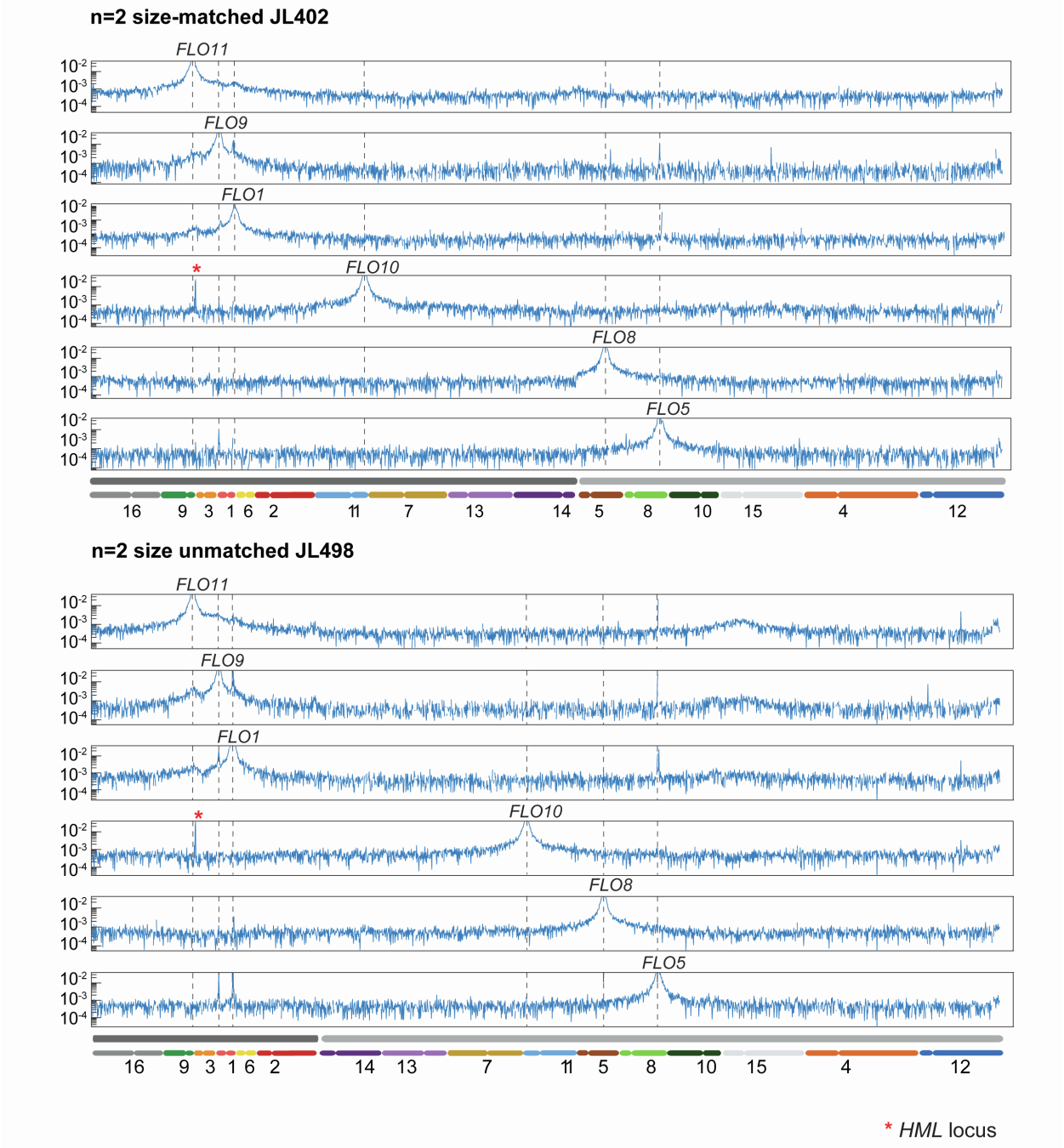

Figure S9, related to Main Figure 2. 4C-like profiles with *FLO* genes as viewpoints.
Each plot shows the contact pattern of a 15 kb window, centered on a single *FLO* locus in n=2 size-matched (JL402 top panels) and n=2 size-unmatched (JL498 bottom panels). Red star indicates *HML* locus.

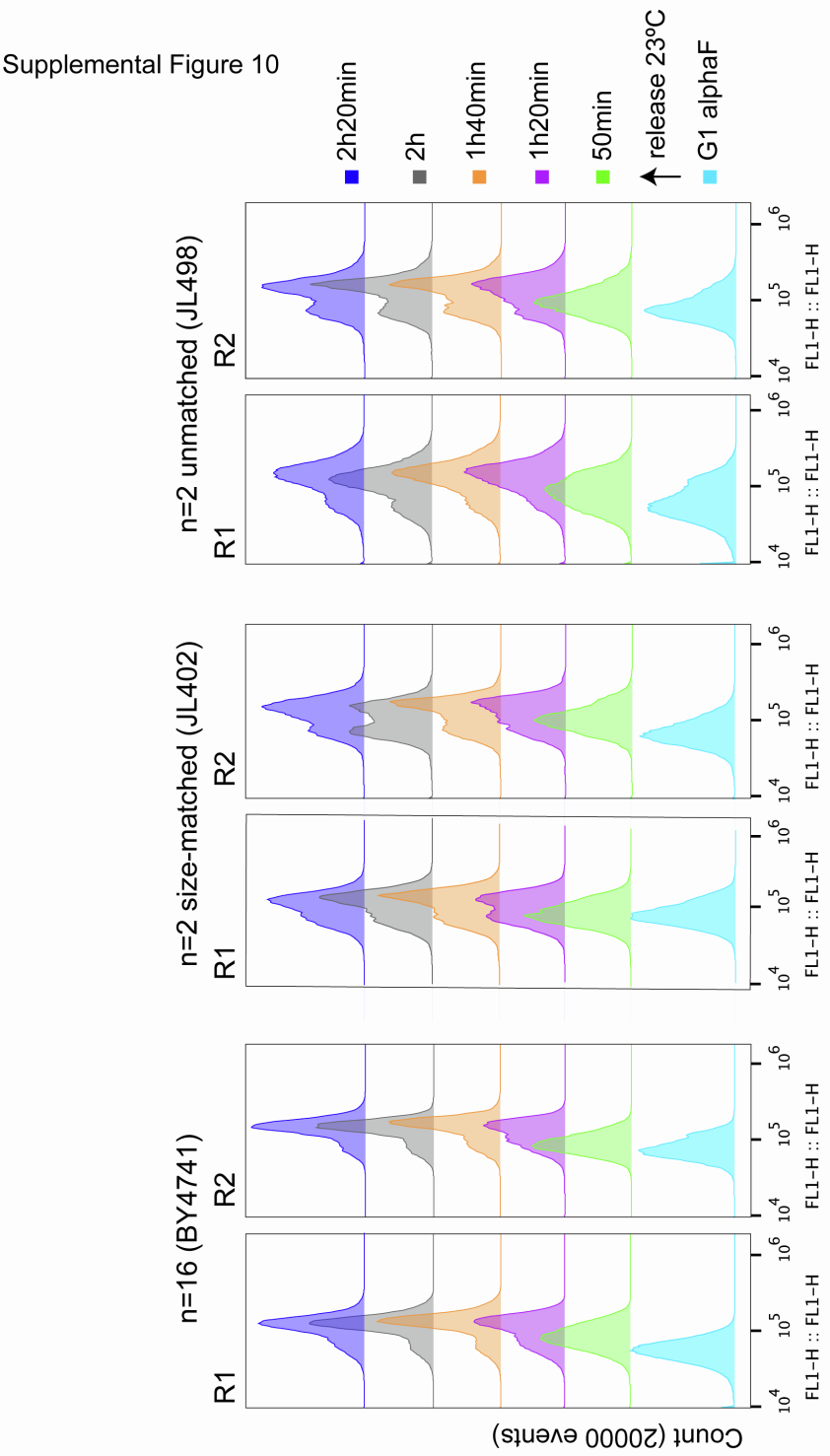

Figure S10, related to Main Figure 3. S-phase progression in n=16 vs. n=2 (JL402 size-matched and JL498 unmatched) strains.

Flow cytometry profiles of DNA content of cells synchronized in G1 with α -factor and release in S phase at 23˚C. Two independent replicates are shown (R1 and R2) for each strain.

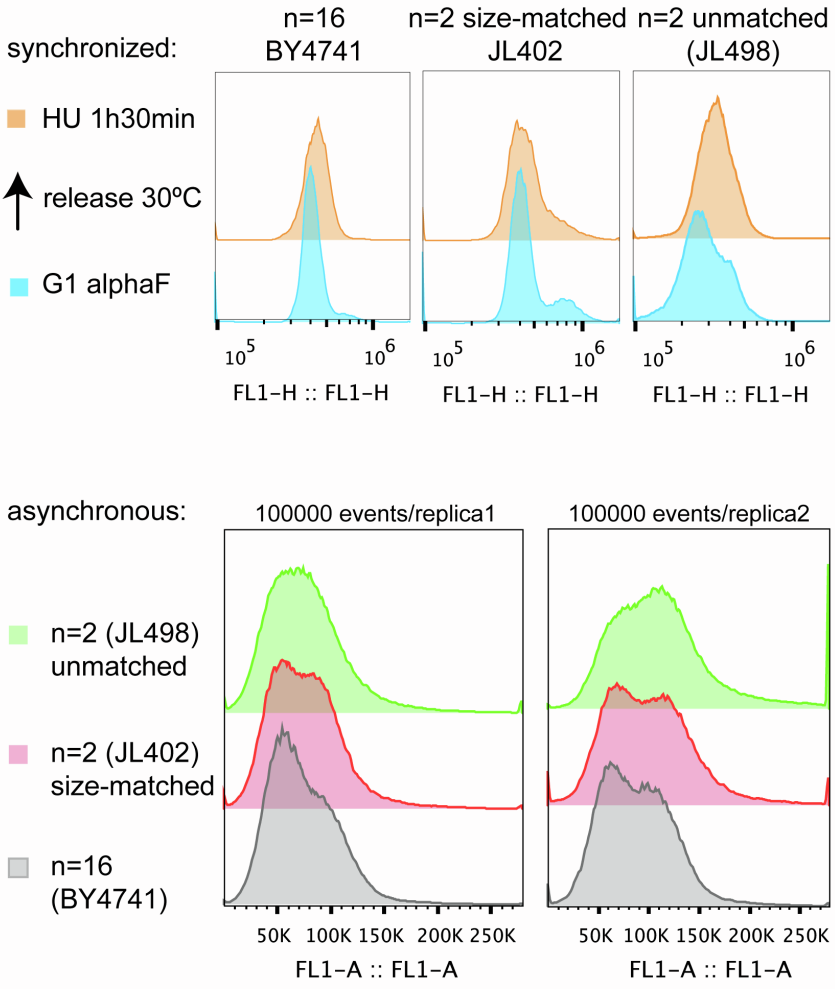

Figure S11, related to Main Figure 3. G1 and S-phase synchronizations of samples used for computing replication firing profiles in n=16 and n=2 (JL402 and JL498).
Top panels: DNA content of cells synchronized in G1 with α -factor, released and arrested in early S phase with HU. Bottom panels: DNA content of asynchronized cell populations.

Figure S12, related to Main Figure 3. Comparison of origin firing profiles in n=2 JL402 vs. n=16 BY4741.

Each profile is the average representation of three independent replicates, showing the sequencing coverage ratio of S phase (HU) synchronized cells normalized on the G1 (α-factor) non-replicating cells. Replication timing profiles (1kb-binned) of n=16 are shown in gray, while those of n=2 are in orange. Inactivated centromeres in n=2 are shown in brackets.

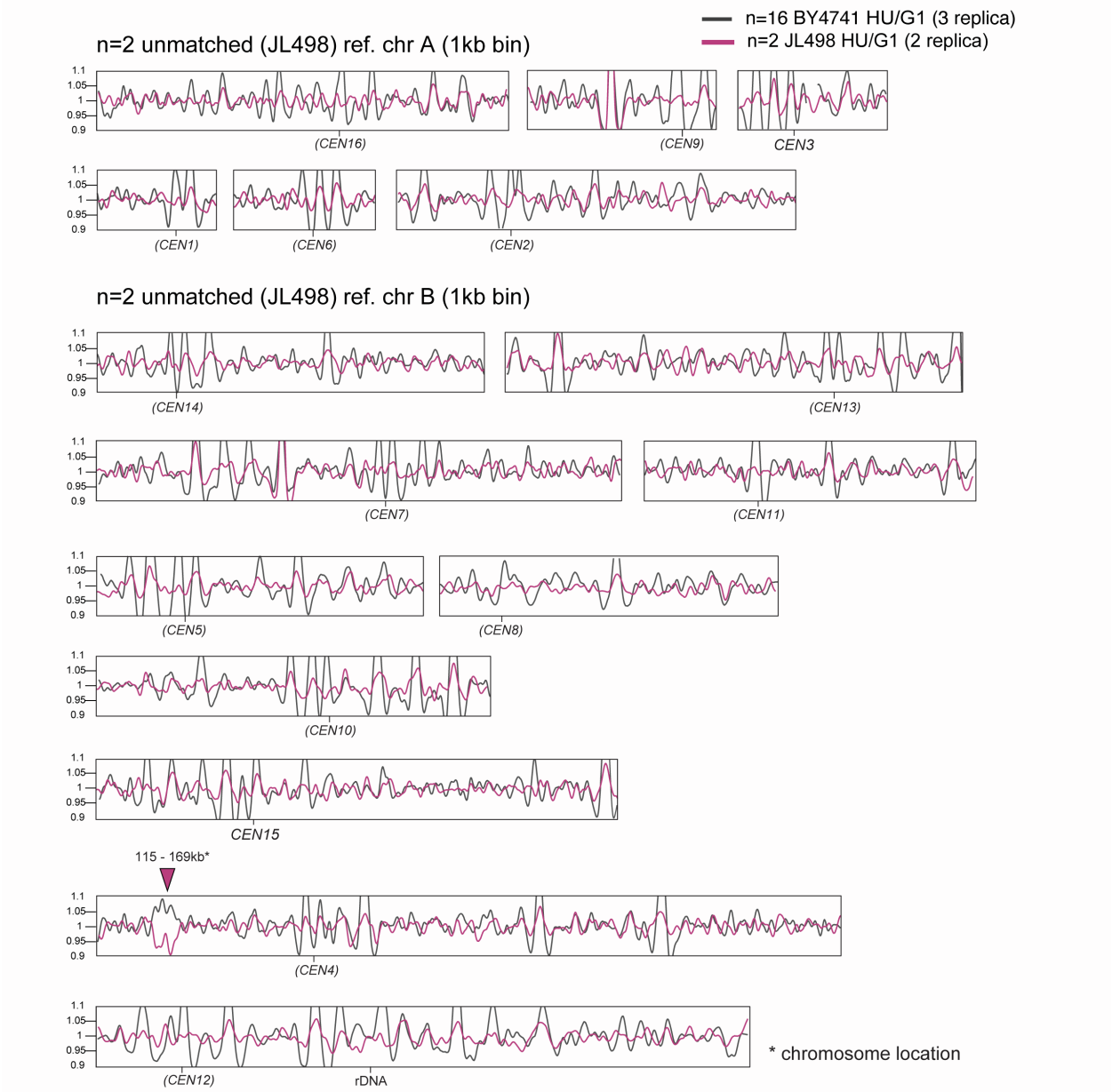

Figure S13, related to Main Figure 3. Comparison of origin firing profiles in n=2 JL498 vs. n=16 BY4741.

Notice that origin firing in n=2 JL498 is overall less distinct compared to n=2 JL402, a result of its inefficient synchronization in G1 (see histograms in B). Arrowheads in C and D point at 3 distinct locations where the replication firing differ between n=2 and n=16. Two of them (on former chr7 and chr12) contain repeated Ty-1 elements (LTR retrotransposon) and appear only in the n=2 size-matched strain. Whereas the 3rd (on former chr4) in coherent in both n=2 strains and is located in a region where none of the manually curated replication studies[55,69,70] identified any origin in ~90kb.

Supplemental Figure 14

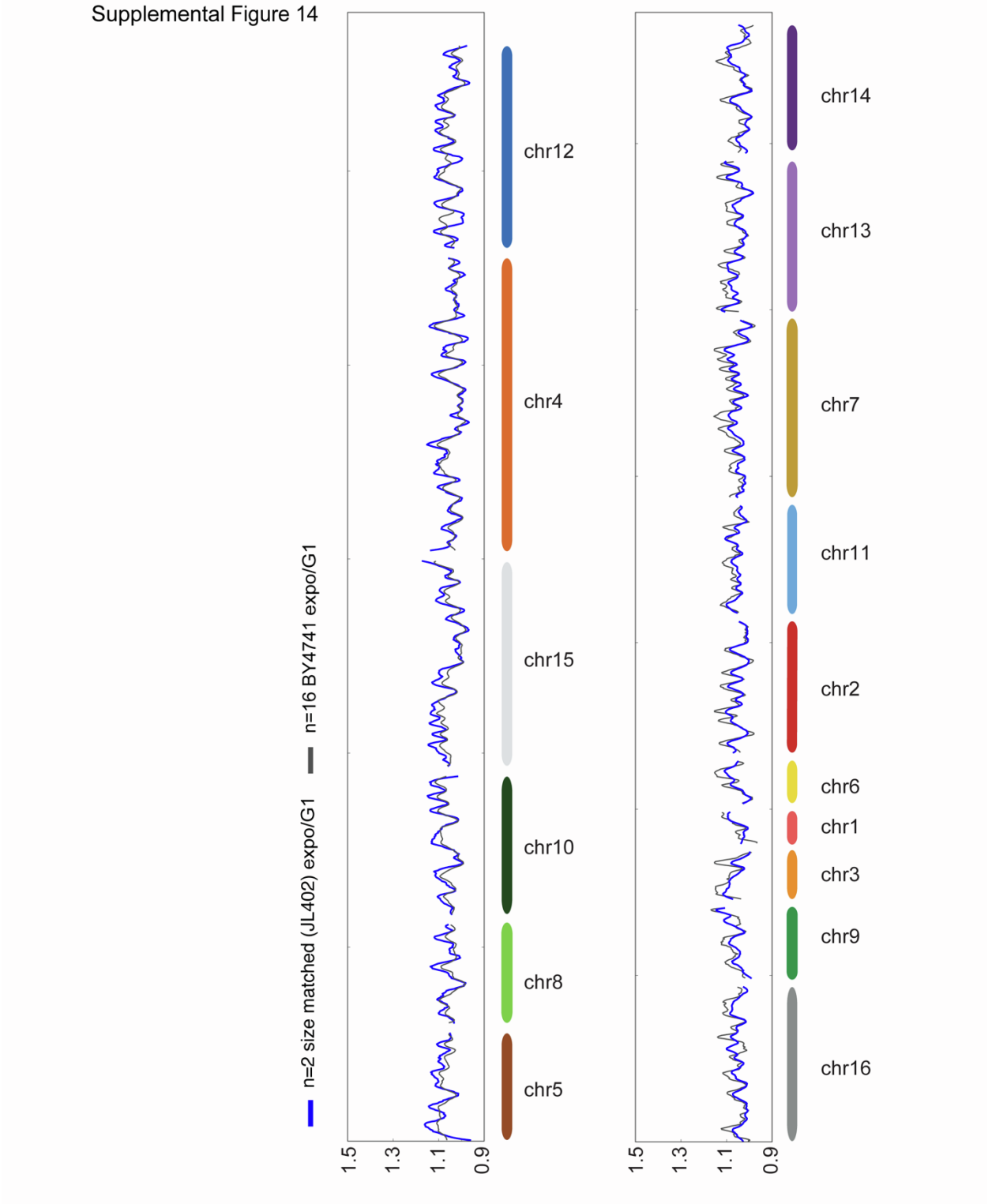

Figure S14, related to Main Figure 3. Comparison of replication profiles of n=2 JL402 vs. n=16 BY4741. DNA replication profiles, binned at 5kb, were computed on exponential growing cells normalized on non-replicating G1 profiles.

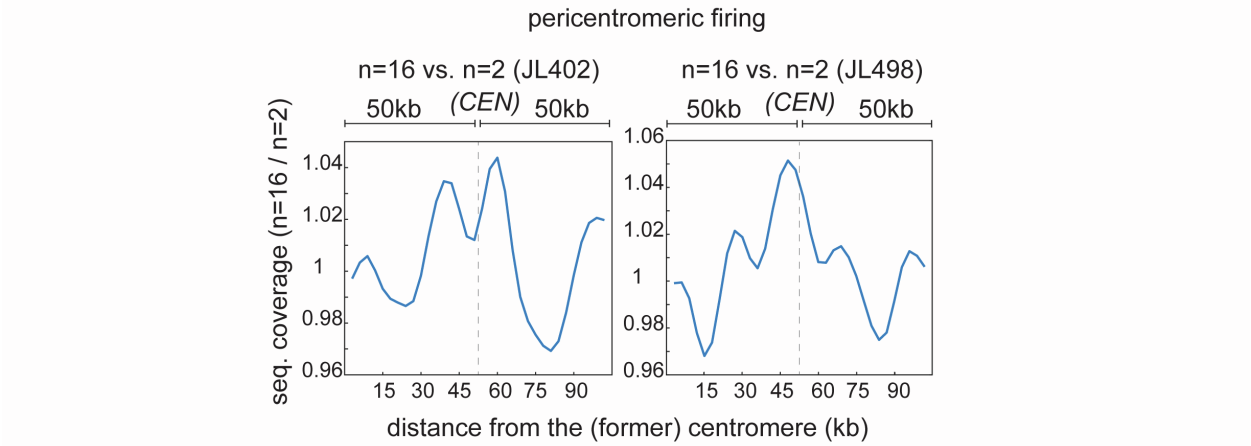

Figure S15, related to Main Figure 3. Inactivated centromeres fire late during S-phase. Pericentromeric firing in n=16 vs. n=2 (JL402 size-matched and JL498 unmatched). Ratio plots show the early firing of pericentromeric regions (~100 kb) in n=16 in respect to n=2, in which centromeres were inactivated. Centromere position is indicated with a dotted line.

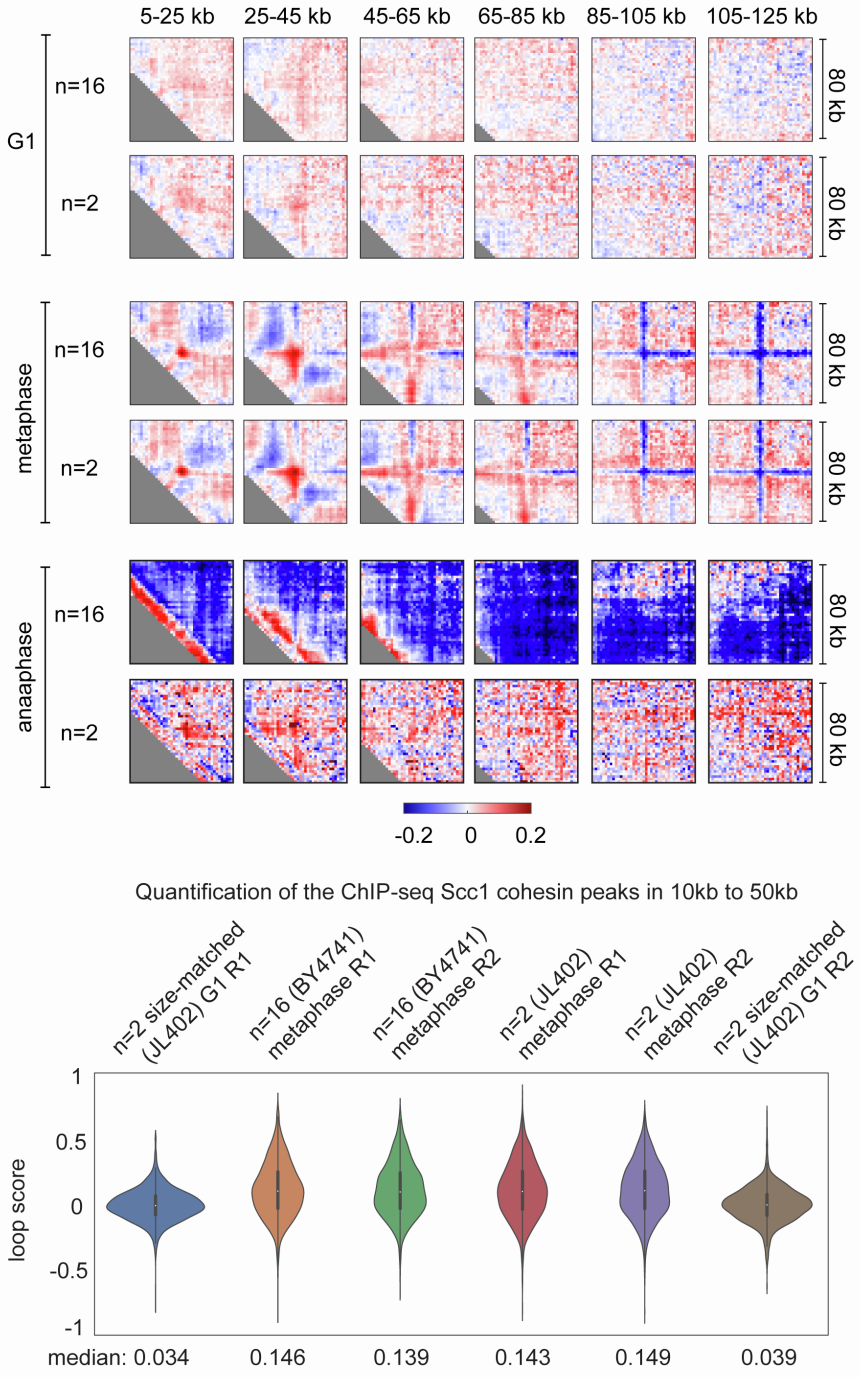

Figure S16, related to Main Figure 4. Cohesin-dependent reorganization of megachromosomes during cell division.

Cumulative log-ratio maps of cohesin-dependent contact enrichment as a function of distance from Scc1 *cis* sites during cell cycle progression: G1, metaphase (nocodazole) and anaphase (*cdc15-2* ts). Blue to red color scale represent an enrichment in contacts dependent on Scc1 in respect to random sites. Violin plots quantify contact enrichment in 10-50 kb windows from Scc1 binding sites in n=16 and n=2 size-matched (JL402).

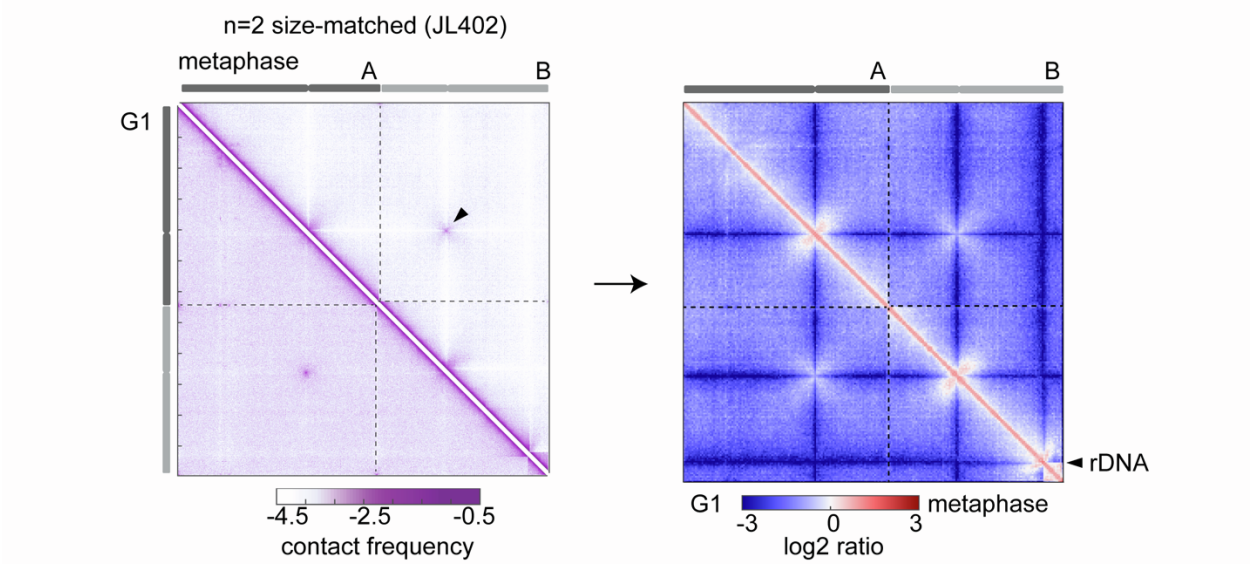

Figure S17, related to Main Figure 4. Contact comparison maps of n=2 (JL402) cells synchronized in G1 and metaphase. Blue to red color scale in the log-ratio map reflects contact enrichment in metaphase compared to G1 (50bk-binned; log2). Black arrowheads indicate inter-centromere contacts.

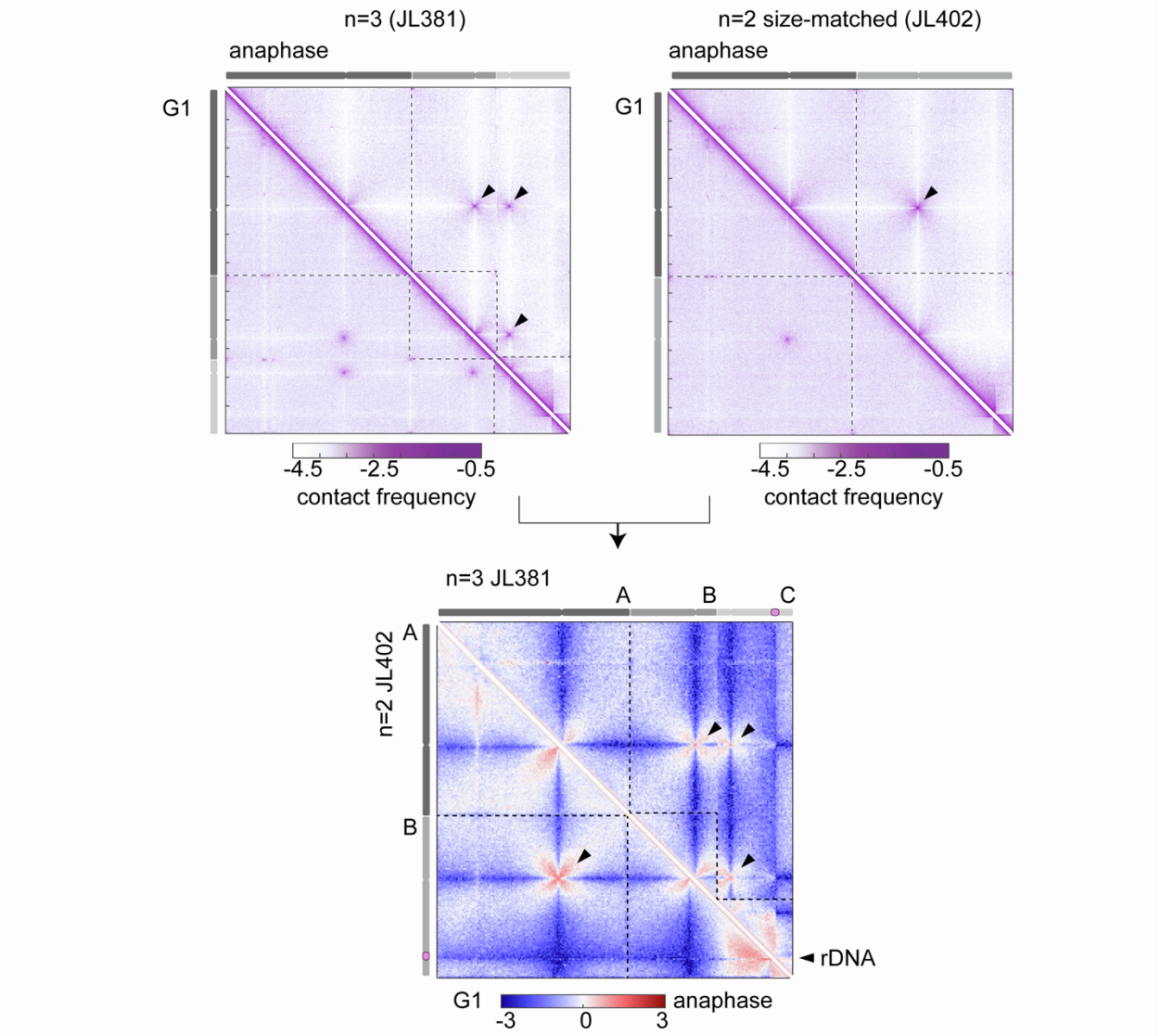

Figure S18, related to Main Figure 4. Contact comparison maps of either n=3 (JL381) or n=2 (JL402) strains synchronized in G1 and anaphase. Blue to red color scale in the log-ratio maps reflects contact enrichment in anaphase compared to G1 (50bk-binned; log2). Black arrowheads indicate inter-centromere contacts.

Table S6, related to Main Figures 1, 2 and 4. Hi-C libraries.

Strain name	Karyotype	Synchronization method	Total paired-end reads	Aligned paired-end reads	Total contacts in map
BY4741 (Lazar-Stefanita et al., 2017)	16	none	43649470	31761165	17649810
BY4741	16	metaphase nocodazole (exp. 1)	31738518	19384914	18264990
BY4741	16	metaphase nocodazole (exp. 2)	27475676	17295275	16137114
JL381	3	none	47645690	36846370	13606005
JL381	3	G1 elutriation	71227924	47667278	14943151
LS381	3	Anaphase *cdc15-2*	32895220	23554200	3173547
JL410	3	none	69886343	55663288	6428681
JL410	3	G1 elutriation	33874272	18479512	13061046
JL402	2	none	31808387	24803480	12993017
JL402	2	G1 elutriation	33942738	26955095	11214102
JL402	2	metaphase nocodazole (exp. 1)	28339485	18963164	17441919
JL402	2	metaphase nocodazole (exp. 2)	26207064	17208531	16102493
JL402	2	Anaphase *cdc15-2* (exp. 1)	49078905	38115942	13116462
JL402	2	Anaphase *cdc15-2* (exp. 2)	30859455	24679199	9090904
JL498	2	none	48557489	38575397	13925428